ELSEVIER

Contents lists available at ScienceDirect

Marine Geology

journal homepage: www.elsevier.com/locate/margo



Deep-water canyon-channel systems of the Queensland Plateau, Northeast Australia

Sebastian Lindhorst ^{a,*}, Linus Budke ^a, Robin J. Beaman ^b, Jan Oliver Eisermann ^a, Christian Hübscher ^c, Niko Lahajnar ^a, Thomas Lüdmann ^a, Jody M. Webster ^d, Christian Betzler ^a

- ^a Institut für Geologie, Universität Hamburg, Bundesstr. 55, 20146 Hamburg, Germany
- ^b College of Science and Engineering, James Cook University, Cairns 4870, Queensland, Australia
- E Institut für Geophysik, Universität Hamburg, Bundesstr. 55, 20146 Hamburg, Germany
- d Geocoastal Research Group, School of Geosciences, University of Sydney, Madsen Building (F09), Sydney 2006, NSW, Australia

ARTICLE INFO

Keywords: Submarine canyons Carbonate drift sediments Seafloor grooves Plunge pools Bottom currents Carbonate platform dismantling

ABSTRACT

Sediment conduits like erosive canyons and channels are common morphological elements of submarine landscapes down to abvssal depths. While canvon-channel systems connected to slopes and shallow water are well studied, detached sediment-routing systems emerging in deeper waters have received less attention, especially in carbonate settings. We study the sedimentary architecture and evolution of an extensive canyon-channel system in the 'Willis Passage', a marine strait between the Magdelaine and Willis carbonate banks (Queensland Plateau, northeast Australia). The canyon-channel system is detached from the slopes of the carbonate banks, emerges at depths of >500 m and runs over more than 100 km towards the slope break of the carbonate plateau. The canyon is several kilometres wide and several tens of metres deep. Morphological edges (knickpoints) occur along the canyon course; one with a plunge pool at its downstream foot wall. Current ripples and coarse-grained lag deposits at the floor of the canyon indicate bottom-current activity and possibly winnowing of fine-grained sediment. The seafloor outside the canyon is intersected by bundles of grooves (linear seafloor cuts), tens of kilometres long. Sedimentological and morphological characteristics indicate that canyon-channel system and grooves are shaped by eastward-flowing bottom currents, which is in a direction counter to the dominant westward-flowing oceanic current regime. We propose that eastward-flowing sediment-laden bottom currents originate from the channelization of oceanic currents by the carbonate edifices of the Queensland Plateau, paired with tidal pumping in the narrow passages between the banks. This mechanism is most efficient during episodes of lowered sea level, while bottom currents are much weaker during sea-level highstand. Our seismic data reveal the existence of buried individual canyon-channel systems and document that the Queensland Plateau underwent episodic changes in the local current regime since the upper Miocene. Based on new geophysical and oceanographic data, as well as video observations of the seafloor, we show that slope-detached deep-water canyonchannel systems act as a conveyor, routing sediment from carbonate platforms to the deep ocean. As a link between the neritic realm and abyssal depths, these systems are important agents of dismantling and degradation of carbonate platforms and underline the role of bottom currents in shaping these depositional environments.

1. Introduction

Erosive canyons and channels are prominent morphological elements of submarine landscapes, from continental shelves and slopes to abyssal depths. While the term canyon describes an erosive landform that has been created by incision and lateral erosion over long periods of time, channels are sediment conduits that at least temporarily carry a considerable amount of sediment in comparison to their dimensions

(Shepard, 1981; Menard, 1955). Channels are common architectural elements of submarine canyons and deep-sea plains and are sometimes considered the sub-aqueous equivalents of terrestrial rivers regarding their morphology and their role in sediment routing (Imran et al., 2007; Peakall, 2015; Peakall and Sumner, 2015; Gardner et al., 2020). Submarine canyon-channel systems are integral parts of sediment source-to-sink conveyors and conduits for sediment transport from shelves to abyssal depths (Wynn et al., 2007; Meiburg and Kneller, 2010; Gardner

E-mail address: sebastian.lindhorst@uni-hamburg.de (S. Lindhorst).

^{*} Corresponding author.

et al., 2020; Heijnen et al., 2022; Peakall, 2015; Peakall and Sumner, 2015; Watson et al., 2017). Sediment transport in some of these systems, for example at the flanks of the Bahamian carbonate banks or downstream of the Mediterranean Outflow, is generated by saline density currents (Habgood et al., 2003; Flood et al., 2009; Peakall and Sumner, 2015). Most shelf- or slope-attached channels, however, are formed by turbidity currents and sediment-laden density flows, triggered by slope failures or shallow-water or riverine sediment input (Wynn et al., 2007; Puga-Bernabéu et al., 2011, 2013; Peakall and Sumner, 2015; Heijnen et al., 2020, 2022). Other processes involved in generating sediment-laden deep-water flows include the resuspension of sediment by contour currents, internal waves, or tidal bottom currents (Shanmugam, 2003; Miramontes et al., 2020; Normandeau et al., 2024).

The focus of most previous research has been on attached canyon-channel systems starting mid-slope or are connected to shallow waters via shelf- or slope-channels (Payros and Pujalte, 2008; Flood et al., 2009; Puga-Bernabéu et al., 2013; Micallef et al., 2014; Peakall and Sumner, 2015; Watson et al., 2017; Mulder et al., 2017, 2019; Counts et al., 2018; Jorry et al., 2020; Heijnen et al., 2020, 2022). Detached sediment-routing systems emerging in deeper waters of 100 s to 1000s of m depth have received considerably less attention (Habgood et al., 2003; Stow et al., 2013; McArthur and McCaffrey, 2018; Gardner et al., 2020; Yu et al., 2022).

We study a deep-water carbonate canyon-channel system and associated submarine landforms from the Queensland Plateau, northern Australia. The canyon-channel system emerges at a low-relief seafloor in depths >500 m and appears detached from the slope sediment-routing system of the carbonate banks. We hypothesize that 1.) sediment transport in this canyon-channel system is active during sea-level low-stands; 2.) canyon formation is driven by a bottom-current flow being opposite to the prevailing oceanic current direction; and 3.) the canyon-channel system act as a conveyor, routing sediment from the platform surrounding towards the deep ocean. We present new geophysical data

and seafloor imagery and examine the morphology and sedimentary architecture of the canyon, its channels, and the surrounding seabed. The most plausible explanations for the formation of this canyon-channel system are determined and it is shown that these canyons represent an important agent in carbonate platform dismantling.

2. Study area

2.1. Geological setting

The Queensland Plateau is part of the East Australian carbonate province in the Coral Sea, which also includes the Great Barrier Reef and the Marion Plateau. The study area encompasses the deep-water passage between Willis and Magdelaine carbonate banks, here termed the 'Willis Passage' (Fig. 1).

The Queensland Plateau was detached from the Australian mainland by the late Cretaceous and presently encompasses about thirty isolated carbonate banks and atolls. These carbonate edifices unconformably overlay a much larger carbonate platform partially drowned in the early Late Miocene, between 13.6 and 12.7 Ma, coeval with the strengthening of the regional bottom-current regime (Mutter, 1977; Davies et al., 1989, 1991; Betzler et al., 1993, 2024a). Development of the modern high-relief carbonate banks in the middle Pliocene (post 3.61 Ma; Betzler et al., 2024a) followed a period where carbonate sedimentation at the Queensland Plateau was characterized by small, low-relief banks, mounds and sediment drifts.

Neritic carbonate production and export is highly dependent on sea level and generally peaks during sea-level highstand (Schlager, 2005). With lowered sea level, bank tops emerge and the neritic carbonate factory is restricted to a narrow zone along the platform slope. Present water depth on top of the carbonate banks in the study area is between 50 and 60 m. During the last glacial period, lagoonal areas were therefore almost continuously subaerial exposed for about 65 kyrs, until

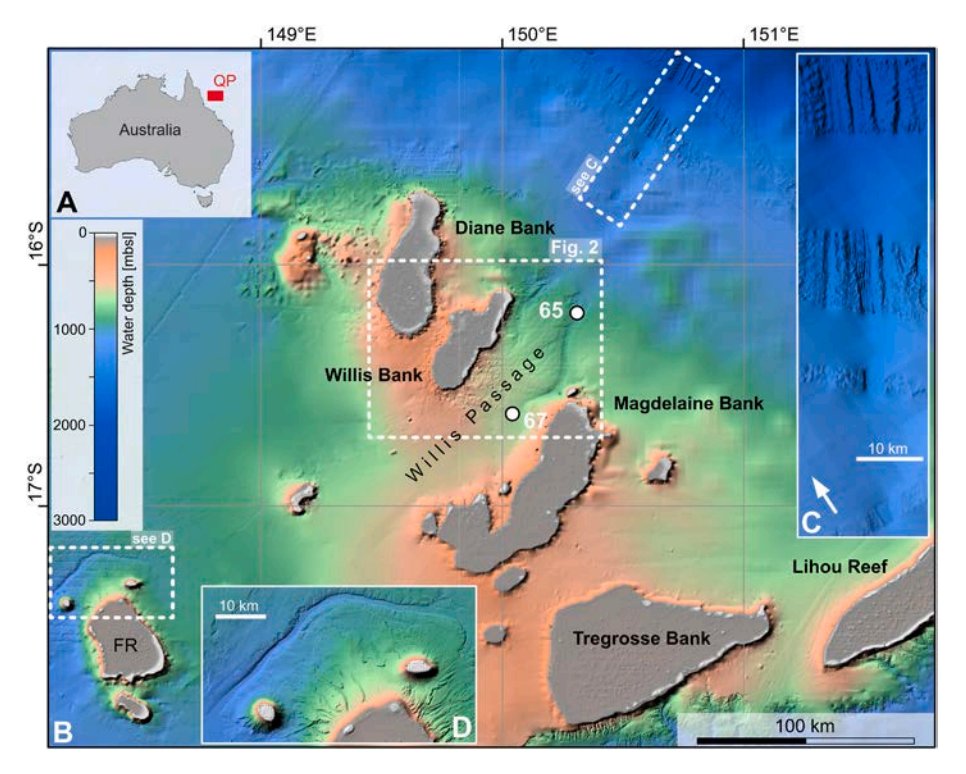


Fig. 1. Overview of the study area. A) location of the Queensland Plateau (QP), northeastern Australia; B) Bathymetric overview of the study area. The marine strait between Willis and Magdelaine banks is referred to as 'Willis Passage'; FR: Flinders Reefs; white circles mark CTD stations SO292-065CTD (65) and SO292-067CTD (67) (see Supplement 3); C) Distal continuation of canyon-channel systems C1 and C2; see text for discussion; arrow points north; D) Westward-draining canyon-channel system north of Flinders Reefs; Bathymetric data used in B, C is from the gbr100 dataset (Beaman, 2010); data used in D is from RV Falkor cruises FK200802 and FK200429 (Brooke, 2020; Beaman and Schmidt Ocean Institute, 2024).

about 10 ka BP, when post-glacial rising sea level flooded the bank edges (Lambeck et al., 2014; Grant et al., 2014; Hinestrosa et al., 2022; Supplement 1). Today, bank tops are covered by extensive *Halimeda* meadows and mounds, while sand cays and small coral reefs line the outer rim of the banks (Fig. 2; Supplement 2). Sea-level highstand carbonate production of the modern carbonate banks of the Queensland Plateau is therefore considered mesophotic, and highstand sediment export from the banks is limited (Orme, 1977; Reolid et al., 2024).

Sediment at the modern seafloor surrounding the carbonate banks is a fine-grained carbonate ooze (Betzler et al., 2022). Major components are planktonic foraminifera, pteropods, and bioclasts, while benthic foraminifera, ostracodes, sponge spicules, as well as few gastropods, otoliths and volcanoclastics in the form of pumice are minor components.

2.2. Oceanography

The trade winds are the main drivers of the surface circulation in the Coral Sea (Wolanski, 1982). The regional oceanic current pattern over the Queensland Plateau, however, is controlled by the South Equatorial Current (SEC; Fig. 3A). When passing the Coral Sea and reaching the Queensland Plateau, the SEC comprises the North Vanuatu Jet (NVJ) and the North Caledonian Jet (NCJ), which both show large seasonality (Schiller et al., 2015; Colberg et al., 2020). The NVJ is a broad, upper thermocline current, whereas the NCJ is narrow and extends to water depths of at least 1500 m (Kessler and Cravatte, 2013). The current system of the SEC bifurcates east of the Queensland Plateau (around 17 to 18°S; Brinkman et al., 2001). As a result, the NVJ flows northwards and forms the Gulf of Papua western boundary current (Andrews and Clegg, 1989; Kessler and Cravatte, 2013; Colberg et al., 2020). The NCJ turns south, enters the Queensland Plateau, and eventually becomes the East Australian Current (EAC; Wyrtki, 1962; Boland and Church, 1981; Church, 1987).

Data from float drifters show that the carbonate banks of the Queensland Plateau are bathed by westward-flowing waters of the NCJ, with maximum speeds of 5 to $11~{\rm cm~s^{-1}}$ (Kessler and Cravatte, 2013 and references therein). No long-term current measurements are available for inter-reef oceanic and tidal currents of the Queensland Plateau, which are expected to be highly influenced by the rugged topography of the banks. Numerical modelling of tidal imprint on surface and upper thermocline currents (down to c. $100~{\rm m}$ of water depth), however, shows a strong semi-diurnal cyclicity of the surface flow in the passages between larger banks, with a primarily west- to south-directed flow and subordinate counter currents (AIMS, Australian Institute of Marine Science, 2024; Sandery et al., 2019). Modelled current velocities in the passages between the banks and atolls fluctuate over the tidal cycle between almost zero and about $0.6~{\rm m~s^{-1}}$ (Fig. 3B).

Water masses in the study area comprise the Tropical Surface Water (TSW, down to approx. 100 m), the South Pacific Tropical Water (SPTW, c. 100–280 m), and the Western South Pacific Central Water (WSPCW; below 280–300 m; Gasparin et al., 2014; Betzler et al., 2022; Supplement 3). Water masses at depths exceeding about 500 m are influenced by the Antarctic Intermediate Water (AAIW). The water is very clear with turbidity in the range of 0.03 to 0.10 NTU (Nephelometric Turbidity Unit; with 3 NTU being equivalent to 1 mg l $^{-1}$). Turbidity is slightly increased near the seafloor; potentially due to sediment resuspension by bottom currents (Betzler et al., 2022). Calculated water density (sigma-theta) increases from 22.5 to c. 26.8 kg m $^{-3}$ down to water depths of 500 m and reaches 27.3 kg m $^{-3}$ at about 1000 m (Supplement 3).

3. Methods

3.1. Multibeam bathymetric data

Multibeam bathymetric data were acquired at a speed of 2.8 to 4.1 m

s⁻¹ (5.5 to 8 kn) using the Kongsberg EM122 swath echosounder of RV Sonne. The EM122 has a nominal frequency of 12 kHz, an angular sector coverage of up to 150°, and beam widths of 1.0° x 0.5°. Equidistant beam spacing and dual swath mode was used for all lines. In general, spatial resolution of multibeam data is governed by sounding density, the acoustic footprint of each sounding, and depth resolution (Mosher, 2011). The EM122 depth accuracy is 0.2 % of depth for inner beams (up to 45° from ship nadir) and increases to 0.6 % of depth for the outermost beams (Kongsberg Maritime, 2011). The cross-track sounding density, determined by the sounding density and the effective acoustic footprint, is assumed to be better than 7 m for water depths of 400 m and better than 18 m for water depths of 1000 m (for angular coverage 140°; Kongsberg Maritime, 2011). The along-track sounding density, dependent on acoustical footprint, cruise speed and ping rate, is about 4 m at depths of 400 m and about 10 m at depths of 1000 m (for dual swath mode and cruise speed of 4.1 m s^{-1}).

Sound-velocity profiles (SVP) and salinity profiles of the water column were obtained from both the CTD measurements and XSV-02 probes (Sippican Inc., Lockheed Martin). Sound profiles throughout the central Queensland Plateau were similar, which implies a uniform water-mass stratification in the area (Betzler et al., 2022).

The software Qimera (v2.4.8, QPS software) was used for processing bathymetric data. Gridded surfaces have cell sizes of 20 m and were created using the CUBE algorithm in Qimera. All bathymetric data were corrected for astronomic tides using tidal predictions with the software AusTides (Australian Hydrographic Office). Tidal predictions for stations 57,845 (Magdelaine Cays) and 57,850 (Willis Islet) were used. Bathymetric data collected by RV Sonne cruise SO292 were supplemented by Kongsberg EM302 multibeam data collected during RV Falkor cruises FK200429 and FK200802 (Brooke, 2020; Beaman and Schmidt Ocean Institute, 2024). Remaining gaps in the multibeam bathymetry were filled for visualisation using the gbr100 dataset (Beaman, 2010), which has a grid cell size of 100 m. For combined multibeam coverage of the bathymetric dataset used for this study see Supplement 4. The bathymetric data were visualized as shaded reliefs to enhance the visibility of the seafloor morphology.

3.2. Parametric sediment echosounder and reflection seismic data

Sub-bottom profiles were recorded using an Atlas Parasound PS70 parametric sediment echosounder with a beam width of 4.5° and a desired secondary low frequency of 4 kHz (see Supplement 4C for spatial coverage of Parasound dataset used for this study). The PS70 was operated in single pulse mode with a transducer voltage of 100 V, and a transceiver amplification of 30 to 40 dB. Sub-seafloor penetration during SO292 was around 10 m on the top of the carbonate banks (water depth around 50–60 m), almost 0 m at steep- and/or lithified parts of the slopes, and 80 to > 140 m in the pelagic sediments surrounding the platforms. Vertical resolution of Parasound data is about 15 cm (manufacturer specifications).

Data were converted to SEG-Y format using the tool ps32segy (Hanno Keil, University of Bremen, Germany). Data processing was performed using the software ReflexW (Sandmeier Software) and comprised data editing, compensation for trace header delay, gain adjustment and along-profile amplitude normalization. Time-depth conversion of Parasound data was done with a sound velocity of 1500 m s $^{-1}$.

Reflection seismic data were acquired using a SeaMUX 144-channel system (Hydroscience Technologies) with an active length of 600 m. The seismic signal was generated equidistantly every 18.75 m by a source array comprising two GI guns with primary volumes of 45 in³ and 15 in³, respectively. The recording length was 4 s with 1 ms sample interval. Processing of seismic data was done using VISTA desktop seismic data processing software (v2021; Schlumberger; for details on acquisition, processing, and extend of seismic dataset acquired during cruise SO292 see Betzler et al., 2022). Effective wavelengths between 10 and 20 m resulted in a realistic vertical resolution of 5 to 10 m. Time-depth

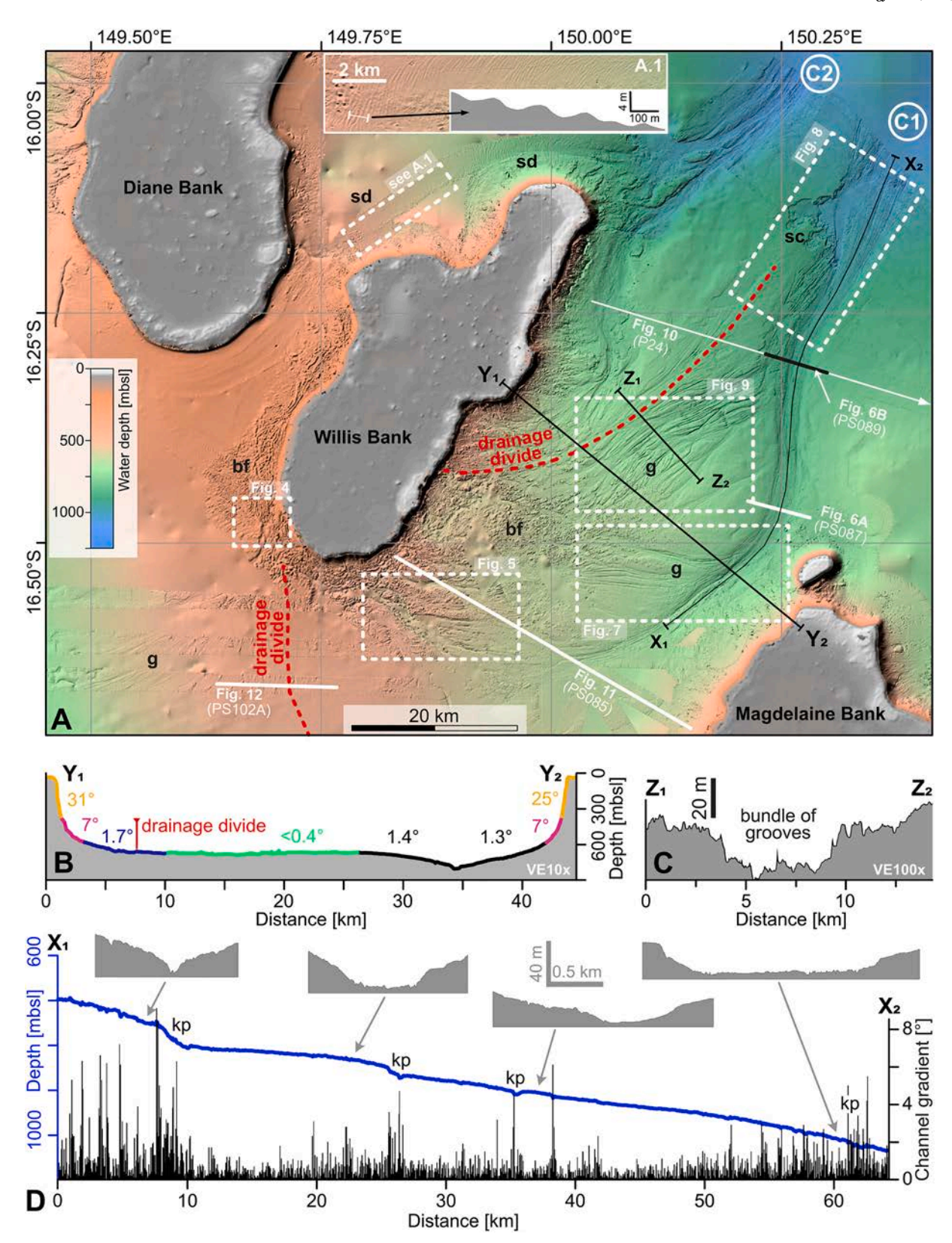


Fig. 2. Details of the study area. A) Bathymetry of Willis Passage and surrounding areas. g: bundles of linear seafloor cuts (grooves); sd: submarine dunes; sc: headwall scarps of submarine landslides; C1, C2: canyon-channel systems mentioned in the text; bf: block field; X, Y, Z: bathymetric profiles shown in B, C, D. Inset A.1 shows submarine dunes north of Willis Bank with a bathymetric cross section. The high-resolution bathymetry is from RV Sonne cruise SO292 and RV Falkor cruises FK200802 and FK200429; data for background bathymetry and bank-top bathymetry are from the gbr100 dataset (see Fig. 1). See Supplement 2 for an unlabelled bathymetric map; B) Bathymetric cross section (Y_1-Y_2) of Willis Passage with maximum slope angles; C) Bathymetric cross section (Z_1-Z_2) of grooves with higher vertical exaggeration; D) Along-channel profile (X_1-X_2) of canyon-channel system C1. Blue line is the bathymetric profile, black bars give the thalweg gradient calculated over 50 m increments; kp: knick points; grey insets show bathymetric cross profiles (view direction is upstream) of the canyon channel system. (For interpretation of the references to colour in this figure legend, the reader is referred to the web version of this article.)

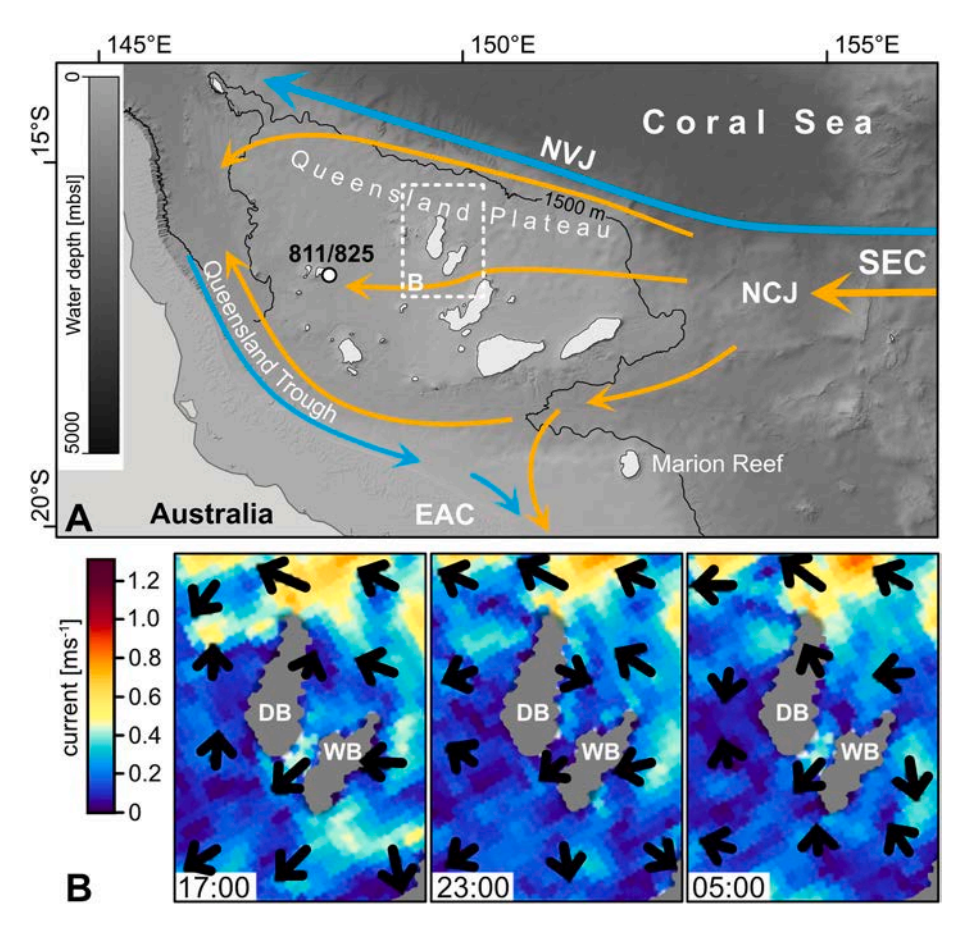


Fig. 3. A) Current regime of the Coral Sea. The 1500 m isobath indicates the Queensland Plateau slope break. 811/825 are ODP Leg 133 Site 811/825; blue arrows indicate upper thermocline currents and orange arrows indicate surface to intermediate (c. 1500 m) currents; SEC: South Equatorial Current; NVJ: North Vanuatu Jet; NCJ: New Caledonia Jet; EAC: East Australian Current. Currents after Kessler and Cravatte (2013); Bathymetric data used is from gbr100 dataset (Beaman, 2010); B) Modelled current direction and velocity at 103 m depth at 6 h intervals 17:00, 23:00, 05:00 for day 2022.07.02/03. Note change in current speed with tidal state in the marine passage between Diane Bank (DB) and Willis Bank (WB). Model results and modified visualisation are from AIMS, Australian Institute of Marine Science (2024). (For interpretation of the references to colour in this figure legend, the reader is referred to the web version of this article.)

conversion was done using a p-wave velocity of 1500 m s $^{-1}$ in the water column and the velocity log and integrated two-way traveltime function of ODP Site 811/825, as provided by Davies et al. (1991). The latter recorded p-wave velocities between 1500 m s $^{-1}$ (at the water-sediment interface) and 2750 m s $^{-1}$ in average (peaks up to 4000 m s $^{-1}$) for the sediment column at depths exceeding 400 m below the seafloor. Depths exceeding the data of Davies et al. (1991) were extrapolated using the traveltime to depth function derived from velocities noted.

3.3. Seafloor imagery

Seafloor imagery data were acquired using the Ocean-Floor Observation System (OFOS) of RV Sonne, a passively towed frame equipped with down-looking video- (Marshal CV350-5X) and still-frame (Canon EOS R5) cameras, and light (Sealite Sphere 5150). The system was lowered to 2–3 m above the seafloor and towed at a speed of up to 0.26 cm s $^{-1}$ (0.5 kn) along a profile line (for details see Betzler et al., 2022). The OFOS position was tracked using iXBlue Posidonia (IXSEA SAS). For scaling, three laser dots were projected equidistantly (40 cm) onto the imaged area. OFOS imagery were also used to generate textured digital outcrop models of the seafloor by means of structure-from-motion algorithms using PIX4D (Pix4D SA). These models are based on series of images obtained along the profile track with large overlap (>60 %).

4. Results and interpretation

4.1. Bathymetry and submarine landforms

The Willis Passage is framed by the carbonate edifices of Willis and Magdelaine banks (Fig. 1). There is an asymmetry in the water depth surrounding Willis Bank: while the marine passage west of Willis Bank, towards Diane Bank, is between 250 and 350 m deep, water depth north of the bank and in the Willis Passage is about 500 to 1000 m (Fig. 2A). The shallowest part of Willis Passage is at its western entrance, where a north-south trending bathymetric high separates the Willis Passage from the western Queensland Plateau. The seafloor west of this bathymetric high is intersected by morphological channels that strike northeast-southwest, while similar features east of the high orient in easterly directions (Fig. 2; Supplement 2). The bathymetric high is therefore referred to as a drainage divide.

Seafloor gradients in Willis Passage are highest at the upper slopes of the carbonate banks (up to more than 30°), decrease to about 7° along the middle and lower slope, and flatten out to values less than 2° at the toe of slopes (Fig. 2B). The bottom of Willis Passage dips with 0.2 to 1.4° towards two northeast-trending canyon-channel systems referred to as C1 and C2. Both canyon systems are separated from each other by another drainage divide and appear detached from the sediment-routing systems of the bank slopes. Bathymetry of the lower-resolution gbr100 dataset (Beaman, 2010) allows following the canyon-channel systems of Willis Passage until the slope break of the Queensland Plateau, a further 130 km towards the northeast (Fig. 1C). With the data available,

however, it remains unclear whether canyons C1 and C2 merge before reaching the edge of the plateau. The studied C1 canyon-channel system of Willis Passage serves as an exemplary model for similar deep-water landforms of the Queensland Plateau. The prominent canyon north of Flinders Reefs at water depths of 900 to 1200 m, which runs west towards the Queensland Trough, is another example (Fig. 1A, D).

The western, southern and south-eastern slopes of Willis Bank are framed by block fields, which extend up to 25 km away from the toe of slopes (Fig. 2). The size of individual blocks reaches 10s to 100 s of m and in general decreases with increasing distance from the bank (Fig. 4). Similar block fields are common around the carbonate banks of the Queensland Plateau and were described as the debris of bank margin failures (Betzler et al., 2024a). Isolated standing blocks in the marine passage west of Willis Bank are surrounded by circular seafloor depressions up to 4 m deep and 80 and 120 m wide. These depressions are interpreted as current scours; i.e. erosional bedforms formed by the acceleration of bottom currents around obstacles and subsequent sediment winnowing (Allen, 1984; Euler and Herget, 2012). While the relative depth of the current scours is constant around the blocks, the adjacent seafloor is about 2 to 4 m deeper on the southern side of the blocks (Fig. 4C). Seafloor photographs from west of Willis Bank show current ripples (decimetre-scale, with sharp crests) that cover the seafloor in between the blocks and scour marks around cobbles and rocks, more pronounced on the southern side of the obstacles (Fig. 4B).

North of Willis Bank, there is a field of submarine dunes, that

migrated along the toe of slope of the bank (Fig. 2A.1). These dunes are about 2 to 4 m high and have wavelengths in the range of 180 to 220 m. While most dune cross sections appear symmetrical, some show an asymmetry pointing either east or west.

The most prominent landform in Willis Passage is the canyonchannel system C1, which emerges south of Willis Bank, crosses the Willis Passage and bends towards the northeast while passing the northern tip of Magdelaine Bank. This canyon is up to several km-wide and several tens of m deep (see canyon cross sections in Fig. 2D). The thalweg gradient of the C1 canyon is 0.14° to 0.35° , which is comparable to other canyons of the Queensland Plateau (canyon C2 has a gradient of 0.3 to 0.4° , the canyon north of Flinders Reef c. 0.2°). The thalweg gradient of canyon C1 locally increases to more than 8° where there are morphological steps in the canyon bed (Fig. 2D). These steps represent an abrupt lowering of the canyon bed, and are therefore seen to resemble knickpoints in the canyon thalweg, following the terminology of Grimaud et al. (2015) and Heijnen et al. (2020).

The seafloor in the area of the emergence of the C1 canyon near the south tip of Willis Bank has a low gradient of $<0.3^{\circ}$ and a very rough relief (Fig. 2). Here, the canyon is 2 km wide and bordered by steep (up to 37°) flanks, which are up to 75 m high and terraced in parts (Fig. 5). In Parasound data, the sediment of the eastern canyon flank appears chaotic, whereas the western flank shows truncated layers. A mounded, elongated well-stratified sediment body unconformably overlies the floor of the canyon. This sediment body is up to 40 m thick, composed of

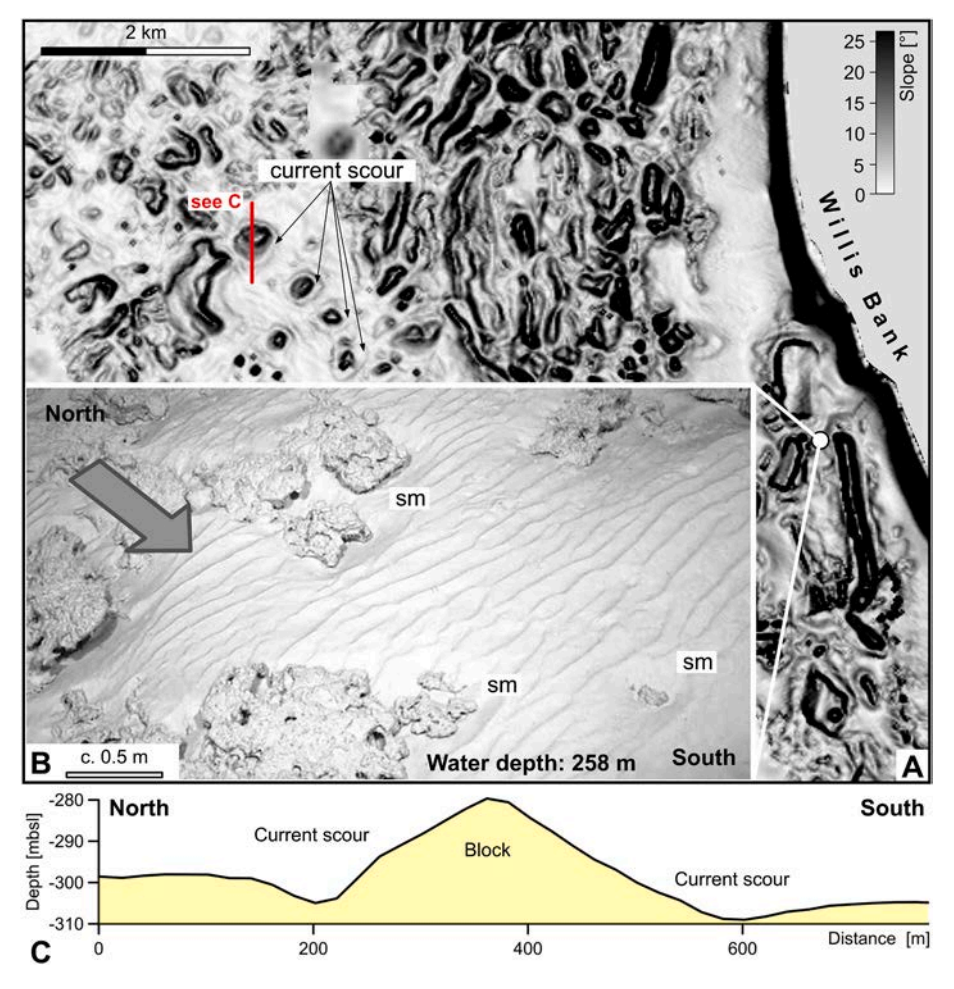


Fig. 4. A) Seafloor morphology west of Willis Bank (Fig. 2 for location). Note current-related circular scours (3 to 5 m deep) around larger blocks (water depth is c. 300 m); B) Seafloor at 258 m with current ripples and current scour marks (sm) around blocks (view is from 3 m above the seafloor). Arrow indicates the assumed bottom-current direction. Image is from RV *Falkor* cruise FK200429, ROV dive 361 (see Beaman and Schmidt Ocean Institute, 2024 for details); C) Topographic profile over one block (see red line in A) based on multibeam bathymetry. Note that the seafloor is lowered on the south side of the block. (For interpretation of the references to colour in this figure legend, the reader is referred to the web version of this article.)

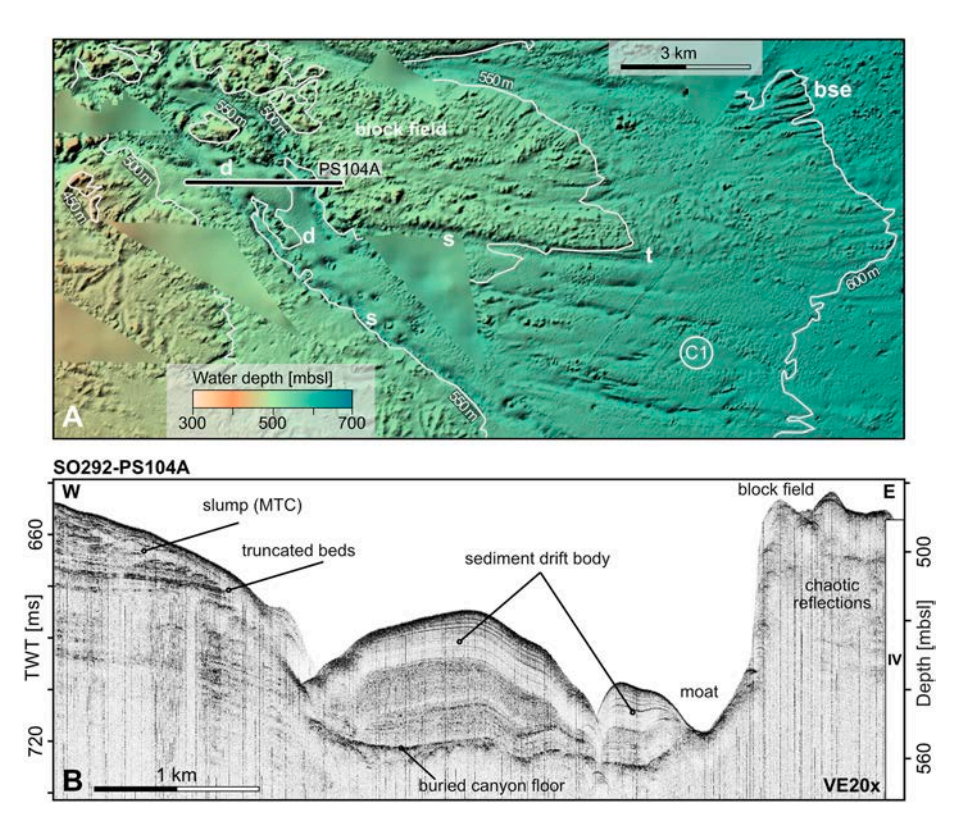


Fig. 5. Area of emergence of canyon-channel system C1 south of Willis Bank (Fig. 2 for location). A) Multibeam bathymetry; s: erosional scarp (up to 75 m high); bse: back-stepping erosion upstream of a scarp; d: drift sediment body. Note linear grooves on the canyon-channel floor; B) Part of Parasound line SO292-PS104A. See black line in A) for location; IV: informal stratigraphic unit (see Fig. 10).

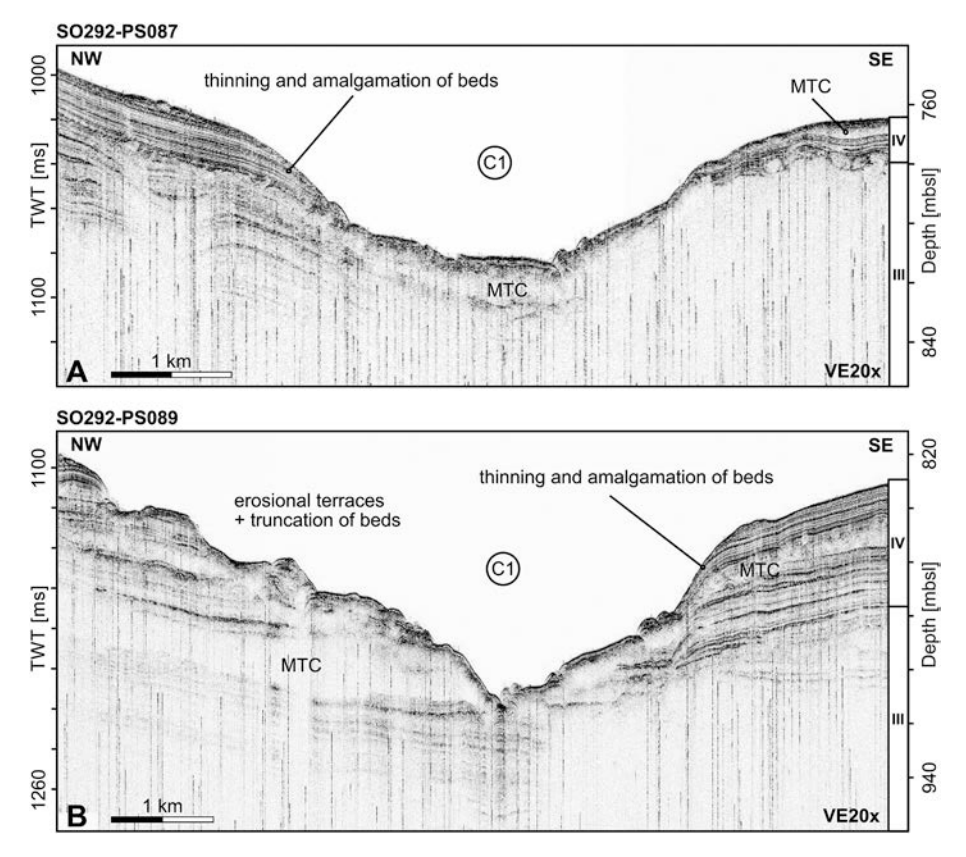


Fig. 6. A, B) Parasound lines SO292-PS087 and SO292-PS089 (Fig. 2 for location). Note erosional terraces and truncation of sedimentary beds on one side of the canyon, and canyon-ward thinning and amalgamation of sedimentary beds on the opposite side. III, IV are informal stratigraphic units (see Fig. 10). MTC: mass-transport complexes; C1: canyon-channel system C1.

convex-upward curved beds, and flanked by channels (Fig. 5B).

The canyon C1 widens down-course and reaches almost 7 km-wide at the eastern limit of the study area (Fig. 2). The canyon is wide and ushaped in cross section in some parts, in others it becomes v-shaped and deeper incised (Fig. 2D). Walls in the outer curve of canyon bends were affected by erosion, as indicated by truncated beds and the presence of erosive terraces (Fig. 6). Canyon inner curves, by contrast, are characterized by a thinning and dipping of sedimentary beds towards the canyon, resulting in an amalgamating stacking pattern. Grooves intersect some segments of the canyon wall (Figs. 7, 8). Parasound data show that these canyon-parallel grooves represent outcropping sedimentary beds (basset edges), which are likely more resistant to erosion than the intermediate layers (Fig. 8B).

Scalloped head scarps left by submarine landslides intersect the seafloor beside the canyon (Figs. 2, 8). These scarps open towards the canyon, are up to 30 m high and have slope angles between 5 and 25°. Similar scarps have been described from carbonate ooze of the Maldives carbonate platform as well as from the southern slope of Tregrosse Bank (Lüdmann et al., 2022a; Betzler et al., 2024a). No talus fans of these landslides are preserved inside the canyon.

The bottom of canyon C1 is intersected by axial channels and linear striations (Figs. 2A, 5A, 7A, 8A). These striations are up to 12 km long, erosively cut up to 8 m into the canyon floor, and in the downstream direction terminate at morphological steps (knickpoints; Figs. 2, 7, 8). OFOS imagery shows that the knickpoints are formed by outcropping sedimentary beds that seem to be at least partly lithified (Fig. 8C). A circular seafloor depression, 5 to 10 m deep and 400 to 500 m in diameter, is present at the foot of one of these knickpoints (Fig. 8A). This depression resembles a submarine plunge pool, a morphological feature well known from seafloor channels elsewhere and proposed to have formed as the result of erosion by sediment-laden flows (Gardner et al., 2020; Mulder et al., 2022). A pronounced axial channel appears downstream of the plunge pool in the C1 canyon. The floor of this channel is covered by ripples and megaripples with wavelengths of c. 0.1 to 0.2 m and up to 1.5 m, respectively (Fig. 8D, E). Patches of coarse

sediment occur near channel walls and in channel bends (Fig. 8F). In OFOS imagery, megaripples appear dark against the channel floor and their sediment seems to be coarse-grained. The resolution of the images, however, does not allow for a determination of components.

The bottom of the Willis Passage outside the canyons is intersected by linear or slightly bent grooves, which start in the distal part of the block field southeast of Willis Bank, largely follow the bathymetric gradient, and merge with the C1 canyon from westerly direction (Fig. 2). Individually they are on average 150 to 180 m wide (maximum c. 500 m) and 8 to 15 m deep, with a v-shaped cross-section and side walls that dip between 8 and 12° (maximum c. 24° ; Fig. 7). The grooves erosively cut into the seafloor as proved by the internal stratification of adjacent ridges, which can be traced from one ridge to the next (Figs. 7, 9; Supplement 5). Grooves are arranged in parallel to sub-parallel running bundles that form shallow channel-shaped depressions, 10 to > 30 m deep (Figs. 2C, 7). Grooves and ridges outside the canyons are covered with a thin (up to 2 m thick) sediment veneer of uniform thickness (Figs. 7C, 9).

The transition zone from the block field to the grooves is characterized by elongated low-relief ridges (Figs. 2, 9). These ridges are often drop-shaped, with tails pointing east. Ridges are 150 to 250 m wide, 1.8 to 2.4 km long (some reach up to 5 km in length), and elevate 5 to 10 m (few up to 25 m) above the bottom of the adjacent grooves. Low-relief ridges flatten out towards the east and grooves become dominant (Figs. 7, 9). Ridges that are morphologically connected to the block field often have one or several blocks at their western termination. These angular blocks are up to several metres large and some show internal bedding in OFOS imagery (Fig. 9C, D). Continuing further east along the ridges, sediment becomes more abundant and covers the blocks (Fig. 9E).

4.2. Stratigraphy

The sedimentary fill of Willis Passage is shown by multi-channel seismic line SO292-P24 (Fig. 10). A strong, irregular reflection forms

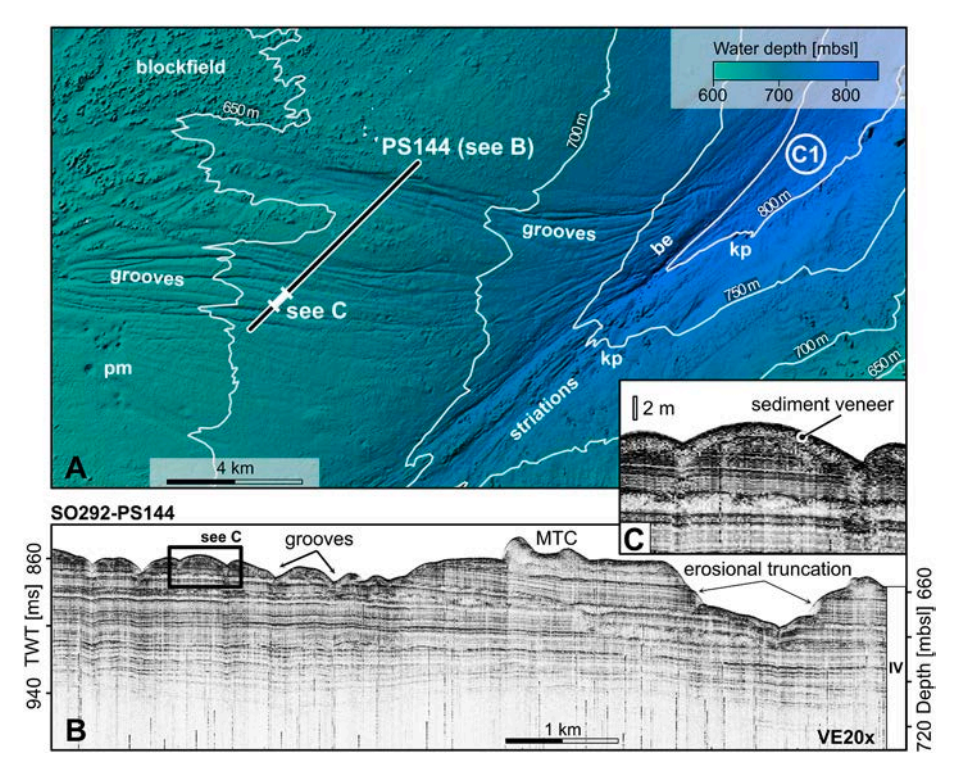


Fig. 7. Bundles comprising linear seafloor cuts (grooves) joining with canyon-channel C1. A) Multibeam bathymetry (see Fig. 2 for location and Supplement 5 for a perspective view); pm: pockmarks; kp: knickpoint; be: basset edges; B) Parasound line SO292-PS144. See A) for location. IV: informal stratigraphic unit (see Fig. 10); C) Detail of B) note the up to 2 m thick sediment veneer that covers grooves and adjacent ridges (scale bar for sediment thickness).

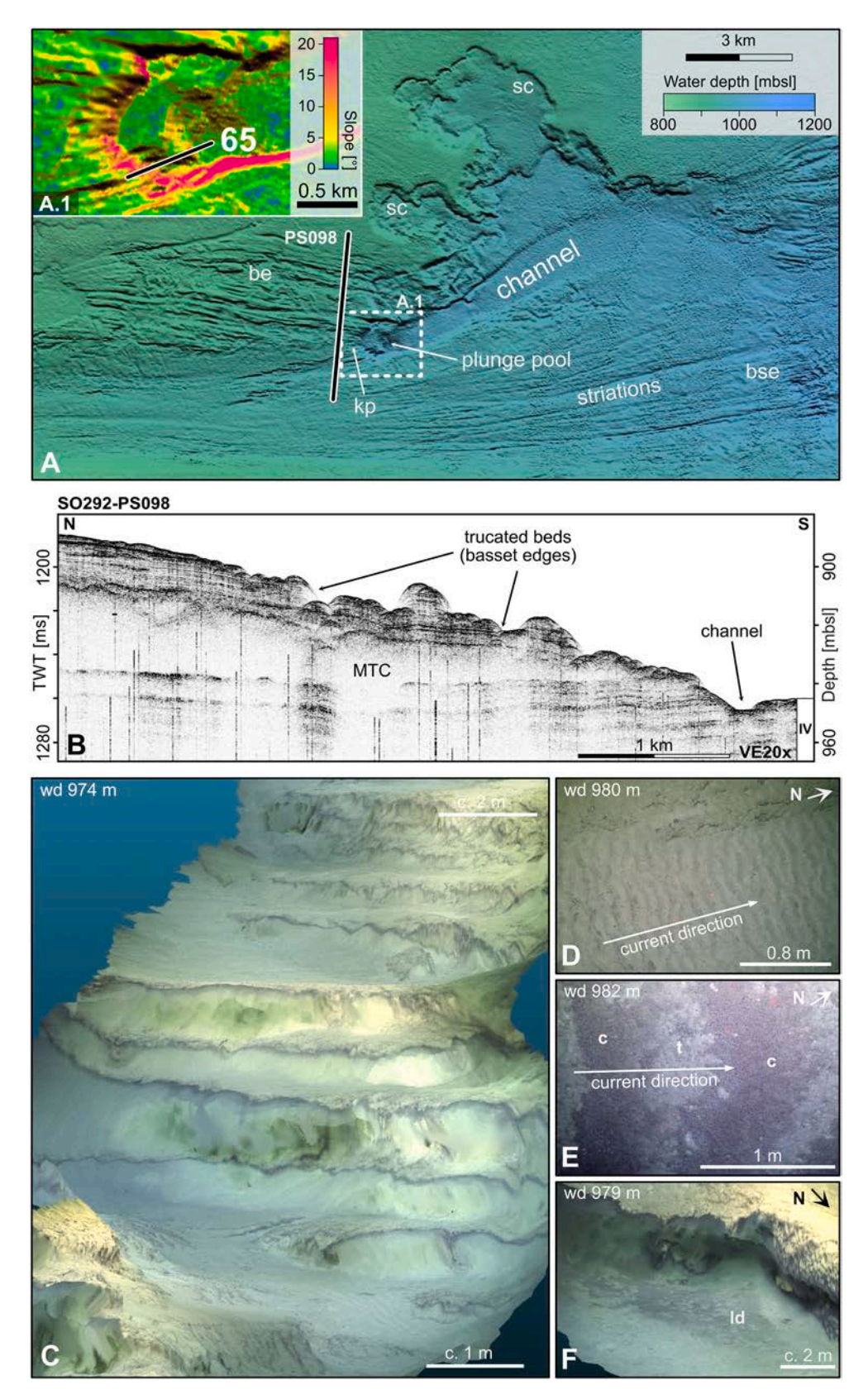


Fig. 8. Details of the lower course of canyon-channel system C1 (Fig. 2 for location). A) Striations at the canyon floor, head-wall scarps of submarine landslides (sc), basset edges (be), back-stepping erosion at a knickpoint (bse), and a plunge pool. Inset A.1 shows a slope gradient map of the plunge pool with location of OFOS-transect SO292-0650FOS (65); B) Parasound line SO292-PS098 which crosses the canyon floor. Hyperbolas are caused by diffraction of the seismic signal at morphological edges; IV: informal stratigraphic unit (see Fig. 10); MTC: mass-transport complexes; C) Perspective view of the up-stream wall of the plunge pool with sedimentary bedding. View is rendered from OFOS photographs (see methods). See A.1 for location of OFOS transect; D, E) Current ripples and coarse-grained

megaripples on the canyon-channel floor down-stream of the plunge pool; t: trough; c: crest; F) Perspective view rendered from OFOS photographs showing a coarse-grained lag deposit (ld) at the foot of the channel wall.

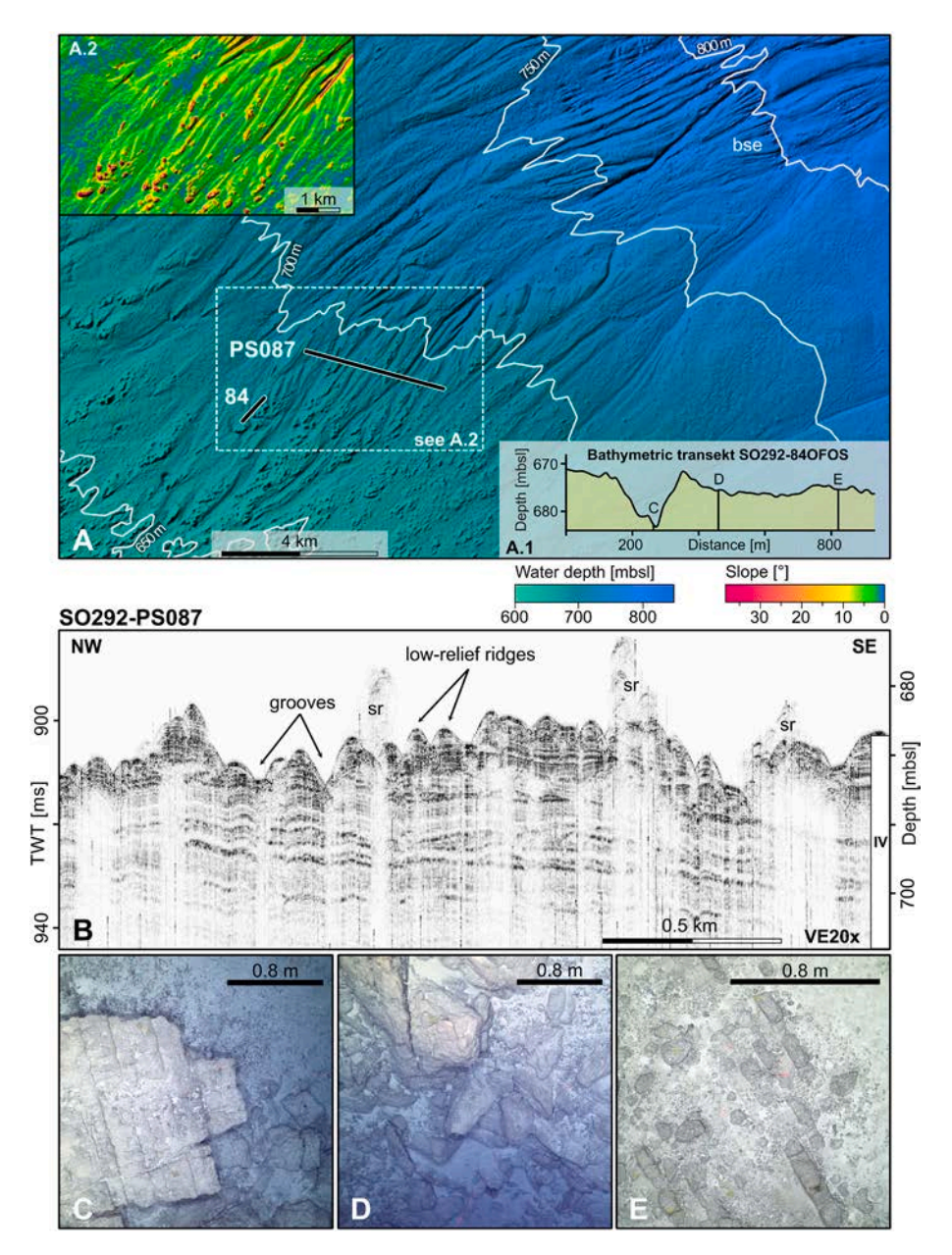


Fig. 9. Erosional bedforms (low-relief ridges and grooves) east of Willis Bank. See Fig. 2 for location. A) Seafloor morphology from multibeam data. 84: OFOS transect SO292-840FOS. Inset profile A.1 shows the morphology along the OFOS transect with positions of seafloor photographs shown in C, D, E; Inset A.2 shows a seafloor gradient map. See white box in A for location; bse: back-stepping erosion upstream of a scarp; B) Part of Parasound line SO292-PS087. Note erosional truncation of sedimentary beds at the flanks of the low-relief ridges. See A) for location of line; sr: side (out-of-plane-) reflections; IV: informal stratigraphic unit (see Fig. 10); C-E) Photographs from OFOS transect SO292-840FOS. C, D) lithic blocks (bedded and fractured) exposed at the seafloor; E) a bedded block covered with fine-grained sediment. For locations see A.1.

acoustic basement of a well-stratified succession at a depth of c. 1900 mbsl (1600–1700 ms TWT, see methods for details on time-depth conversion). The acoustic basement correlates with the top of the Paleozoic (upper Carboniferous to lower Permian) metasedimentary/metavolcanic basement of the Queensland Plateau as drilled in ODP Site 133, holes 924 and 925B (Feary et al., 1993; Shaanan et al., 2018). The sedimentary succession overlying the acoustic basement is about 1100 m thick and comprises sub-horizontal to slightly upward-curved strata that can be traced over several tens of km. These are marine sediments associated with the development of the Queensland carbonate province

since the middle Eocene (Mutter, 1977; Davies et al., 1989, 1991; Betzler et al., 1993). The lateral continuity of these sediments, with horizons traceable over tens of km, points to the lateral uniform deposition in a pelagic to hemipelagic marine setting.

The sedimentary succession of Willis Passage is subdivided into four seismo-stratigraphic units, based on acoustic facies and subsurface geometries (Fig. 10, Units I to IV). The lowermost interval (Unit I, c. 1400 to 1900 mbsl) is characterized by horizontal strata of lateral continuity which pinch out at the paleoslope of Willis Bank. In the second interval (Unit II, c. 1400 to 1000 mbsl), sedimentary beds are gently upward-

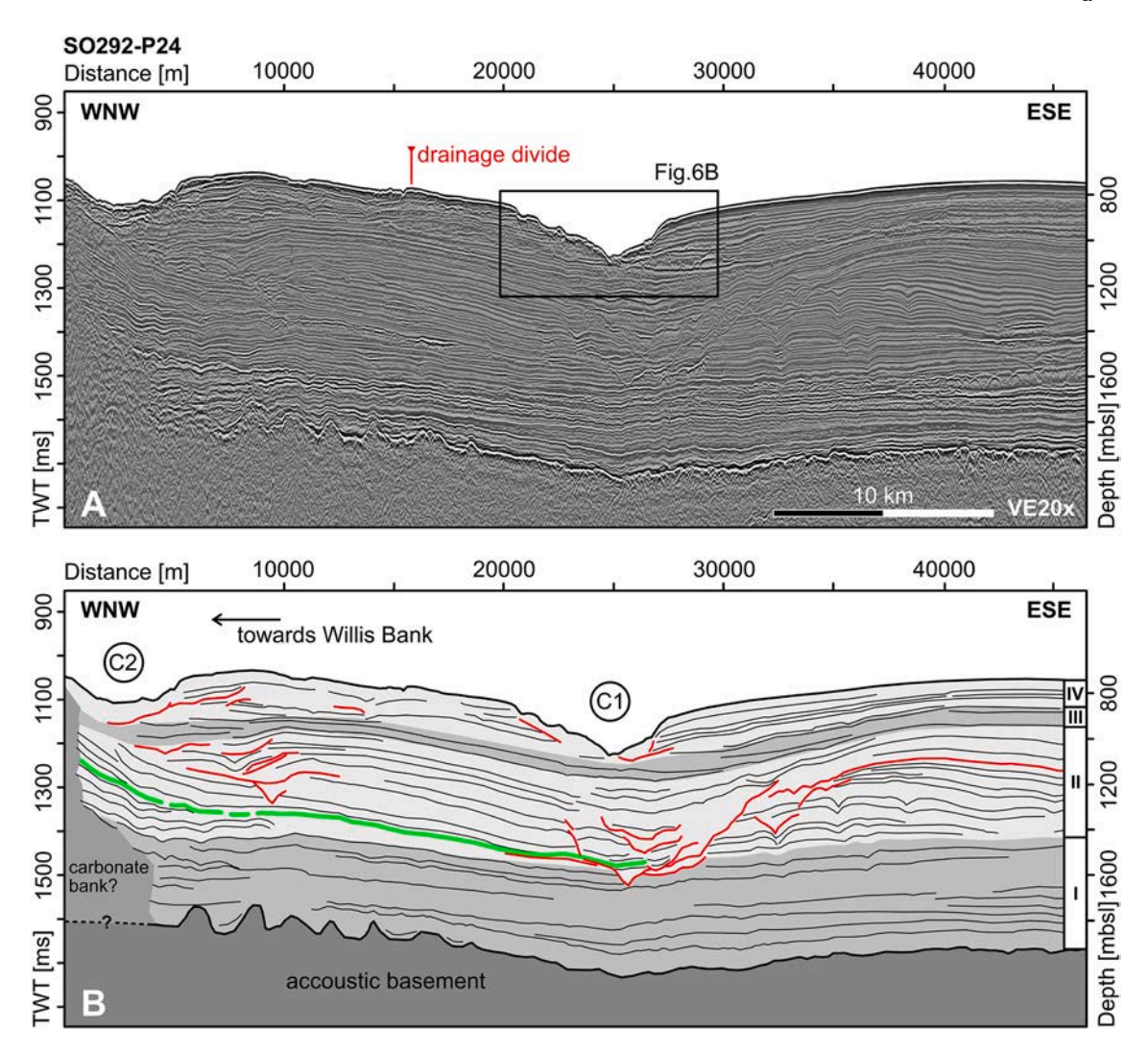


Fig. 10. A) Multi-channel seismic line SO292-P24 cross-cutting Willis Passage. See Fig. 2 for location; B) Interpretation of A). C1, C2: canyon-channel systems C1 and C2; I to IV are informal stratigraphic units; black lines are seismic horizons and red lines trace unconformities; the green line is the seismic horizon correlated with ODP Leg 133, Site 811/825 stratigraphy (age 8.1 to 5.53 Ma); see Supplement 6 for seismic correlation and text for discussion. (For interpretation of the references to colour in this figure legend, the reader is referred to the web version of this article.)

curved and often truncated by low-angle unconformities. This architecture is interpreted to resemble current reworking of pelagic sediment, i.e. drift sedimentation, as this is common in similar marine passages elsewhere (Mullins et al., 1980; Rebesco et al., 2014; Lüdmann et al., 2022b). A large cut-and-fill structure, up to 10 km-wide, is present in Unit II near the centre of the line. The eastern flank of this structure is erosive, as indicated by truncation of beds. The western flank is much less clearly defined and the cut-and-fill structure interfingers with horizontal strata that continue towards the west. Smaller cut-and-fill structures are present in the same stratigraphic interval, further towards the west, near the modern Willis Bank. These cut-and-fill structures are seen to represent a buried canyon-channel system, similar in size to the present-day one. The third interval (Unit III, c. 1000 to 850 mbsl) comprises horizontal strata in absence of cut-and-fill structures. The uppermost interval (Unit IV, c. 850 mbsl to the seafloor) is incised by the C1 and C2 canyon systems, which truncate the horizontal strata of this unit.

More detailed information on the architecture of the younger sedimentary succession comes from Parasound line SO292-PS085, which traverses the western part of Willis Passage (Figs. 2, 11). Data show well-stratified strata that gently dip towards the axis of the C1 canyon. Embedded into these strata, there are several km-large sediment bodies, which have an irregular outer shape and are internally acoustically

transparent (Fig. 11B). The base of these sediment bodies is erosive as indicated by the truncation of sedimentary beds. Sedimentary bodies with similar acoustic facies are common in Parasound data from elsewhere on the Queensland Plateau and were recognized as mass-transport complexes (MTCs; Betzler et al., 2022, 2024a, 2024b). Other erosional structures of Unit IV comprise a more than 2 km-wide and up to 20 m-deep cut-and-fill structure, buried at a depth of about 20–30 m below the present seafloor. The erosional base of this structure cuts into the well-bedded deposits of Unit III and can be laterally traced over more than 8 km. Smaller erosional truncations are present a few metres below the seafloor. These wedge-shaped cut-and-fill structures, each up to 10 m deep and up to 200 m wide, are covered by acoustically more transparent sediments, and are likely buried grooves (Fig. 11B).

The sedimentary architecture of the north-south trending drainage divide south of Willis Bank is imaged in Parasound line SO292-PS102A as well as in seismic line SO292-P27 (Fig. 12; Supplement 6). Seismic and Parasound data show an eastward-directed progradational stacking pattern of sedimentary beds in the upper part of the succession while strata at greater depth indicate a westward progradation of the sedimentary body (Fig. 12; Supplement 6C). Wavy reflections at the limit of spatial data resolution resemble submarine dunes, while sediment bodies with a chaotic internal stratification are mass-transport complexes (Fig. 12 A.1).

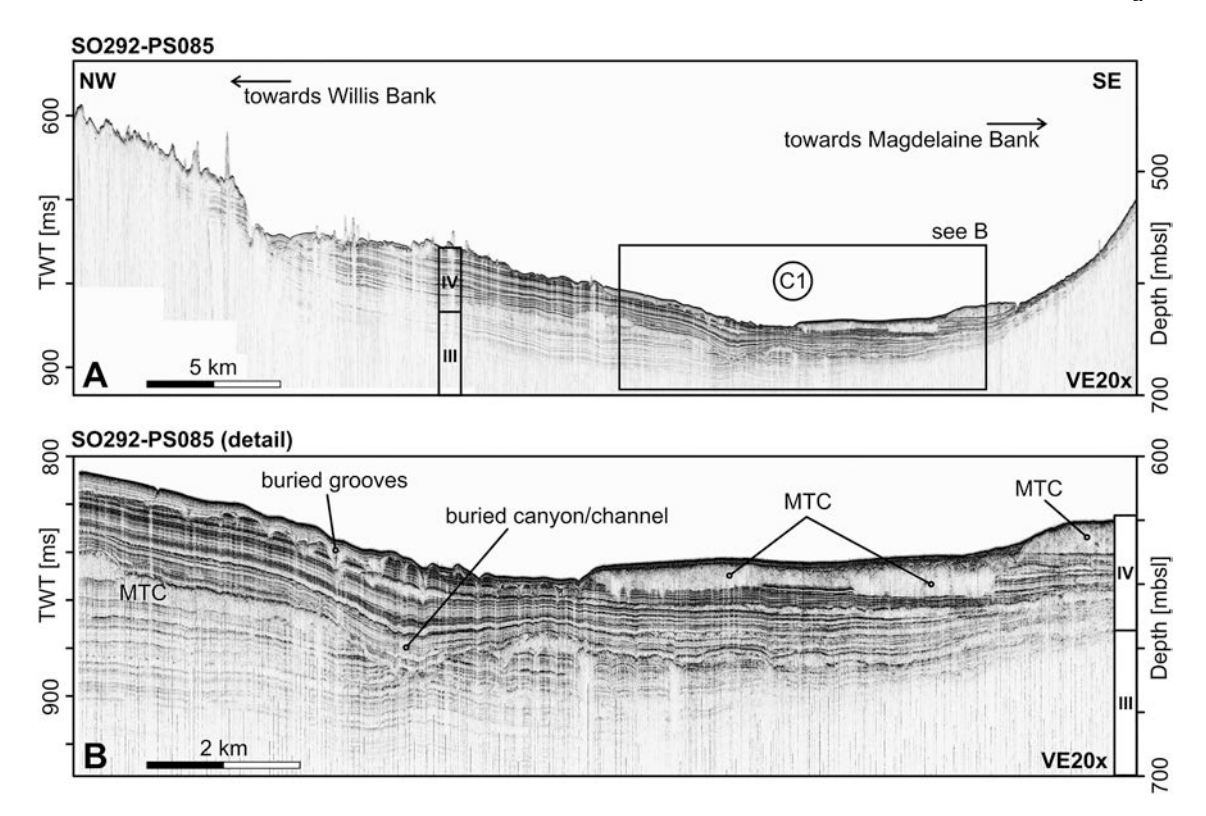


Fig. 11. A) Parasound line SO292-PS085. See Fig. 2 for location. III, IV are informal stratigraphic units (see Fig. 10); C1: canyon-channel system C1; B) Detail of A. Note cut-and-fill structures interpreted as a buried canyon/channel and buried grooves (linear seafloor cuts). MTC: mass-transport complexes.

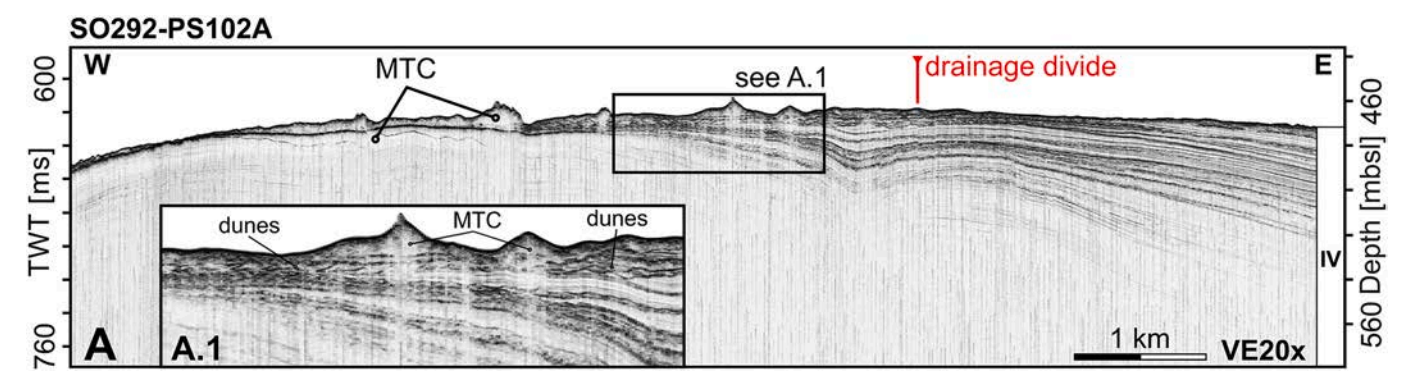


Fig. 12. Part of Parasound line SO292-PS102A which crosses the drainage divide south of Willis Bank. Note divergent stacking pattern of the sedimentary beds, which indicates an eastward-directed progradation of the sediment body. IV is an informal stratigraphic unit (see Fig. 10). See Fig. 2 for location and Supplement 6 for the corresponding multi-channel seismic line SO292-P27.

5. Discussion

5.1. Erosive submarine bedforms in Willis Passage

Linear erosive bedforms are common in Willis Passage. Grooves cut into the floor of the central passage and the side walls of the canyon, while kilometre-long striations intersect the canyon floor (Figs. 2, 7, 8A, 9). These features are interpreted as furrows, as defined by Flood (1981) as linear depressions, eroded into the seafloor by bottom currents. Furrows similar in size to the grooves in Willis Passage, with lengths of up to 10 km, are described from siliciclastic settings, e.g. the Gulf of Cádiz contourite system, and attributed to flow velocities $>0.3~{\rm m~s^{-1}}$ for muddy sediments, and 0.75 to 1.5 m s $^{-1}$ for sandy and coarser sediments (Hernández-Molina et al., 2006; Stow et al., 2009). Deep-water furrows (up to 10 m deep and 50 m wide) with lengths of up to 50 km are reported from the Gulf of Mexico (Bryant et al., 2005). These bedforms

were formed by bottom currents with velocities exceeding 1 m s $^{-1}$. Furrows formed under lower flow velocities (0.05 to 0.2 m s $^{-1}$) were reported from hemipelagic carbonate muds (Flood, 1983 and references therein). Furrow initiation in muddy sediments is seen to be triggered by obstacles that locally enhance seafloor erosion (Flood, 1981). The process of furrow growth has been suggested to represent a feedback loop (Flood, 1981, 1983), where the topography of the furrow bedform induces a secondary helical circulation to bottom-currents, which then results in deepening and linear lengthening of the erosive structure.

Linear erosive bedforms in Willis Passage, however, are only partly explained by the genetic model suggested by Flood (1981). These grooves appear connected to the block fields south of Willis Bank. The large debris potentially caused the vorticity in bottom-current flow typically associated with furrow initiation. The low-relief ridges situated at the transition of the block field to the grooves, however, consist of sediment left in the current shadow of the blocks, as indicated by ridge-

internal strata that are truncated at the flanks of the ridges (Figs. 7, 9). This architecture does not fit with the furrow model which builds on direct erosional incision behind the obstacles. Further, erosional structures in Willis Passage are not straight, but slightly curved, and bundles of grooves form low-relief depressions (Fig. 2C). When merging with the C1 canyon, grooves bend and eventually run along the canyon wall (Figs. 7, 8). Parasound data show that these grooves at the canyon wall are likely basset edges, sculptured by different degrees of erosion of unconsolidated and more consolidated sedimentary intervals. Apparent bending of grooves towards the canyon axis likely is a geometric effect caused by the steepening gradient of the seabed near the canyon and the dip of the sub-horizontal layers. While linear erosion due to local turbulence in the bottom-current flow cannot be ruled out for the grooves that have formed in the direct vicinity of the low relief ridges, the downstream continuation of the grooves appears to be controlled rather by the subsurface lithology than by simple linear extension of the erosive bedforms. In result the grooves in Willis Passage are seen to trace the stratal heads of potentially lithified sedimentary beds. It fits with this interpretation that grooves are arranged in bundles that form shallow depressions in the seafloor, which cut through sub-seafloor sedimentary beds at different burial depths (Figs. 2C, 7).

Striations (linear seafloor cuts) at the canyon floor terminate in downstream direction at morphological steps, which are interpreted as knickpoints (Figs, 2, 7, 8). The formation of these erosional bedforms is seen to be linked to this steepening of the thalweg gradient, which locally enhances the flow velocity. In result, such striations at the canyon floor likely form by retrogressive (back-stepping) erosion, upstream of knickpoints (Gardner, 1983).

Erosion also takes place downstream of knickpoints as a result of increased turbulence due to expansion of the flow when passing the hydraulic jump and/or excavation by the impacting sediment-laden flow (Lee et al., 2002; Bourget et al., 2011). This is where the plunge pool in the C1 channel formed (Fig. 8). Local increase in erosional potential is further indicated by the erosive channel downstream of the plunge pool. Bedforms (ripples and megaripples) and coarse sediment in the outer bends of the channel provide further evidence of bottomcurrent flow and sediment transport in this channel, eventually paired with a winnowing of fines (Fig. 8D-F). Bedforms, similar in size to the ones imaged in the C1 channel, form at current velocities exceeding c. $0.1-0.2 \text{ m s}^{-1}$ (ripples) and 0.4 m s^{-1} (megaripples; Stow et al., 2009). Very low shear velocities in the range of $1.0 \text{ to } 1.8 \text{ cm s}^{-1}$ are needed to entrain fine-grained carbonate particles, and substantial erosion of calcareous ooze takes place at velocities well below 20 cm s⁻¹ (Southard et al., 1971; Prager et al., 1996; Black et al., 2003). Presently, bedforms and lag sediments in the canyon-channel system of Willis Passage are not covered with sediment. An occasional weak flow in the channel appears therefore likely.

5.2. Bottom-current directions

The current regime of the western Coral Sea, including the Queensland Plateau, is mainly controlled by the westward-flowing waters of the South Equatorial Current (SEC), down to depths of 1500 m, and the easterly trade winds, that control the surface currents (Fig. 3A).

In contrast to the regional dominance of westward-flowing ocean currents, sedimentological bottom-current indicators in the study area

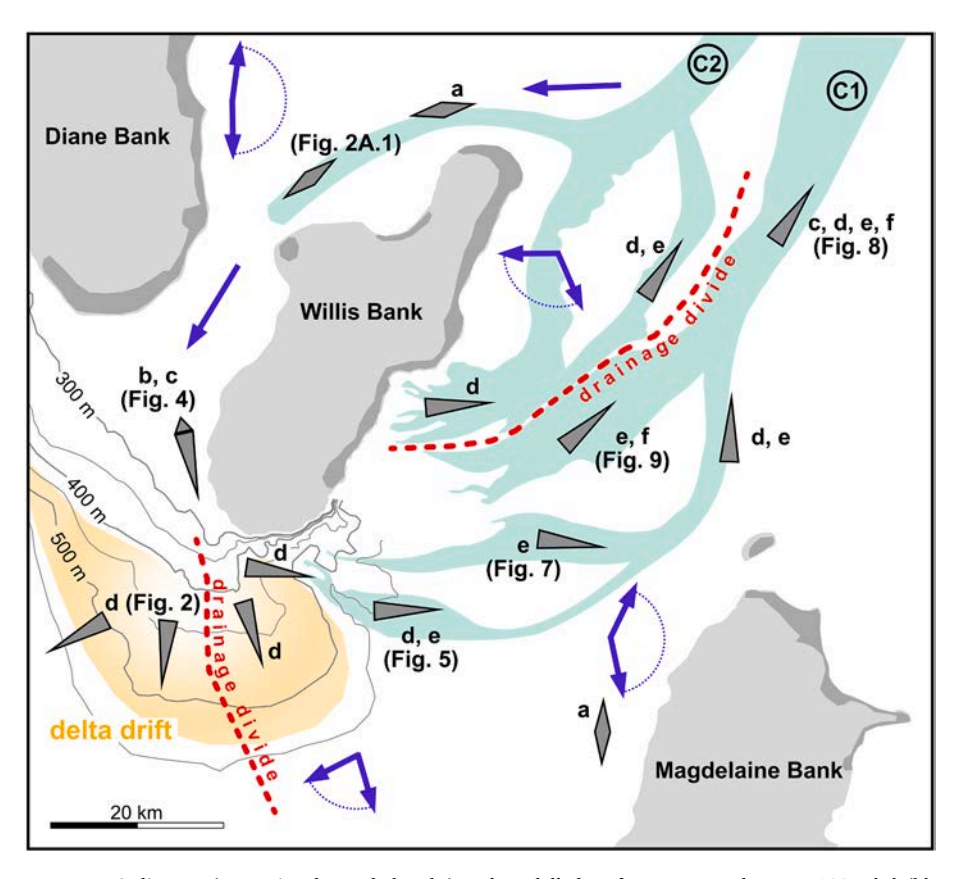


Fig. 13. Sedimentary bottom-current indicators (grey triangles and rhombs) and modelled surface currents down to 103 mbsl (blue arrows; data from AIMS, Australian Institute of Marine Science, 2024). Blue dashed arcs indicate change in surface current direction over one tidal cycle. Bottom current indicators are as submarine dunes with a predominant symmetric cross section; b: current scours; c: current ripples and megaripples; d: canyons and channels; e: grooves; f: drop-shaped low-relief ridges. Canyon-channel systems C1, C2 and connected grooves are marked as green areas. Note that isobaths south of Willis Bank appear to trace the contours of a south-prograding drift deposit (orange area; see text for discussion). For details on surface morphology see figures referred to. (For interpretation of the references to colour in this figure legend, the reader is referred to the web version of this article.)

reveal a complex flow pattern (Fig. 13). The field of submarine dunes north of Willis Bank comprises bedforms that are indicative for both, westward- as well as eastward sediment transport (Fig. 2A.1). Bottom-current indicators in the marine passage west of Willis Bank comprise current scours around blocks and current ripples (Fig. 4). While the circular scours around blocks indicate rotary or multidirectional current directions (Allen, 1984; Euler and Herget, 2012), their asymmetry in cross sections point to the predominance of a net south-directed bottom-flow west of Willis Bank. This view is corroborated by the south-migrated current ripples imaged at similar water depths of around 260 m (Fig. 4B).

A south-directed sediment transport in the passage west of Willis Bank is also indicated by the seafloor morphology south of the passage, which trace a fan-shaped sediment body that appears to prograde in a southerly direction (Fig. 13). Here, grooves at the seafloor point to south-westerly to south-easterly sediment transport, diverting at the local drainage divide (Fig. 2; Supplement 2). The internal architecture of this sediment body is poorly imaged due to the lack of north-south crossing hydroacoustic lines. West-east oriented Parasound data show a shift from westward to eastward progradation of the sediment body with time (Fig. 12; Supplement 6C). In three dimensions, this pattern can be explained by an overall southward progradation. The fan-shaped sediment body south of Willis Bank is, therefore, interpreted as a broad delta drift, i.e. a sediment body accumulated by the deceleration of currents when leaving a marine passage (Lüdmann et al., 2018).

Hydrodynamic models indicate semi-diurnal oscillating, i.e. tidally influenced, currents at a water depth of about 100 m in the passage between Willis and Diane banks (AIMS, Australian Institute of Marine Science, 2024; Fig. 3B). The modelled current velocity varies with a periodicity of six hours between zero and about 0.6 m s⁻¹, while the current remains directed south. Given the low shear velocities needed for the entrainment of carbonate ooze (Southard et al., 1971; Prager et al., 1996; Black et al., 2003), southward-directed bottom currents in the passage are potentially strong enough to resuspend fine-grained carbonate sediment at the toe of the bank slope. In this regard, it is worth noting that oceanographic data acquired during cruise SO292 indicate slightly increased values for water turbidity near the seafloor (Betzler et al., 2022; Supplement 3). This observation only gives a snapshot, but the amount of suspended sediment in near-bottom water masses potentially rose when sea level was lower, e.g. during the last glacial, when water depth in the passage west of Willis Bank decreased to less than 150 m (Lambeck et al., 2014; Grant et al., 2014; Hinestrosa et al., 2022; Supplement 1). Under these circumstances bottom-current velocities are expected to have been higher compared to today, not only due to the lower sea level, but also because of the reduced flow crosssection of the passage, which further focussed the flow.

Bottom-current indicators in Willis Passage include the general orientation of the canyon-channel systems, the orientation of the grooves, and the shape of the low-relief ridges (Fig. 13). All of these features are indicative of a bottom flow that followed the bathymetric gradient towards the east and northeast. Inside the canyon, eastward transport is obvious from striations at the canyon floor, the geometry of knickpoints and associated plunge pools, axial channels, and the shape of sedimentary bedforms like ripples and megaripples.

The further course of sediment-laden flows entering Willis Passage from the west is likely controlled by gravity, as this has been proposed e. g. for calciclastic deep-water channels at the Line Islands Ridge in the central Pacific Ocean (Gardner et al., 2020). In this regard, it is interesting to note that the average volumetric sediment concentration of gravity-driven siliciclastic turbidity currents is estimated to be just a few percent in maximum, with potentially higher concentrations at the sediment-flow interface (Konsoer et al., 2013; Peakall and Sumner, 2015). Low amounts of resuspended sediment are therefore sufficient to drive a down-slope sediment flow. An eastward-directed gravity-driven flow inside Willis Passage appears further likely as the increase in watermass density at depths greater than 500 m is neglectable (Betzler et al.,

2022; Supplement 3), potentially allowing the flow to nest at the seafloor over long distances. This relation not only explains how the flow keeps its erosional potential for several tens of km inside Willis Passage and then beyond towards abyssal depths, but potentially also the observation that low-gradient canyon-channel systems of the Queensland Plateau exclusively develop at greater water depths, i.e. where water density remains largely constant.

The counter-clockwise bottom current around Willis Bank, as documented by the submarine landforms, is suggested to result from current modulation around the carbonate edifices of the Queensland Plateau. In this scenario, the carbonate banks act as obstacles, diverting the westward-flowing water masses of the North Caledonian Jet, with currents being focused and accelerated in the southward-narrowing passage north of Willis Bank. The latter is corroborated by the hydrodynamic modelling of the near-surface currents in the Queensland Plateau that show a strong semi-diurnal tidal cyclicity in flow speed in the Passage between Willis and Diane banks (AIMS, Australian Institute of Marine Science, 2024; Fig. 3B). Similar tidal currents, superimposed on oceanic currents, are known to accelerate the current flow in small marine passages, leading to 'tidal pumping' and unidirectional sediment transport (Saruwatari et al., 2013; Børve et al., 2021). Modelling of currents in the narrow marine passages of the Orkney archipelago (north Scotland), for example, shows a significant increase of the velocity of tidal currents (up to a factor of five times; Saruwatari et al., 2013). Tidalinduced currents are also well known to influence sedimentation in deep water, including submarine canyons, where tidal waves trigger currents strong enough to resuspend sediment (Shanmugam, 2003; Bailey et al., 2024; Normandeau et al., 2024).

5.3. Glacial-interglacial dynamics of the Willis Passage canyon-channel system

During sea-level highstand, as at present, there is a reduced neritic carbonate production on the mesophotic bank tops (Reolid et al., 2024; Fig. 14A). In result, sedimentation around the banks originate from mainly pelagic sources. The erosional grooves in Willis Passage appear inactive at present, as indicated by the sediment veneer that covers grooves and ridges with uniform thickness (Fig. 7C). At the same time, bedforms in the canyon are not covered with sediment (Fig. 8D-F). This observation indicates a (recurring) flow in the canyon at least fast enough to winnow fine-grained pelagic sediment. Bottom currents in the Willis Passage during sea-level highstand are therefore assumed to be weak but not completely interrupted.

With falling sea level, there is a period of increased neritic production on the bank top, when water depth decreases and light availability at the seafloor improves. This peak in shallow-water production is in line with observations from Tregrosse Bank, where neritic sediment export and cross-slope sediment transport are found to intensify during early stages of sea-level fall (Betzler et al., 2024a; Reolid et al., 2024). During these phases of transition, elevated neritic production and intensified wave abrasion on bank tops and upper slopes create a sediment pulse towards the slopes (Fig. 14A).

With the continued fall of sea level, the bank tops become subaerially exposed and neritic production ceases (Fig. 14B). At the same time, bottom currents are expected to accelerate and foster sediment resuspension at the lower slopes of the banks. Now, at the latest, the canyon-channel system of Willis Passage is assumed to be fully active, nourished by sediment-laden bottom currents that flow around the southern tip of Willis Bank and then follow the bathymetric gradient of Willis Passage towards the northeast, routing sediment towards the deep sea. The resulting shift of depocenters, from the toe of bank slopes towards the bank-distal abyssal plain, makes these canyon-channel systems an important element of the carbonate source-to-sink system.

With glacial termination and sea-level rise, bottom currents and sediment transport in the canyon cease. A pelagic sediment veneer starts to drape the canyon and the grooves. When reaching the bank top, the

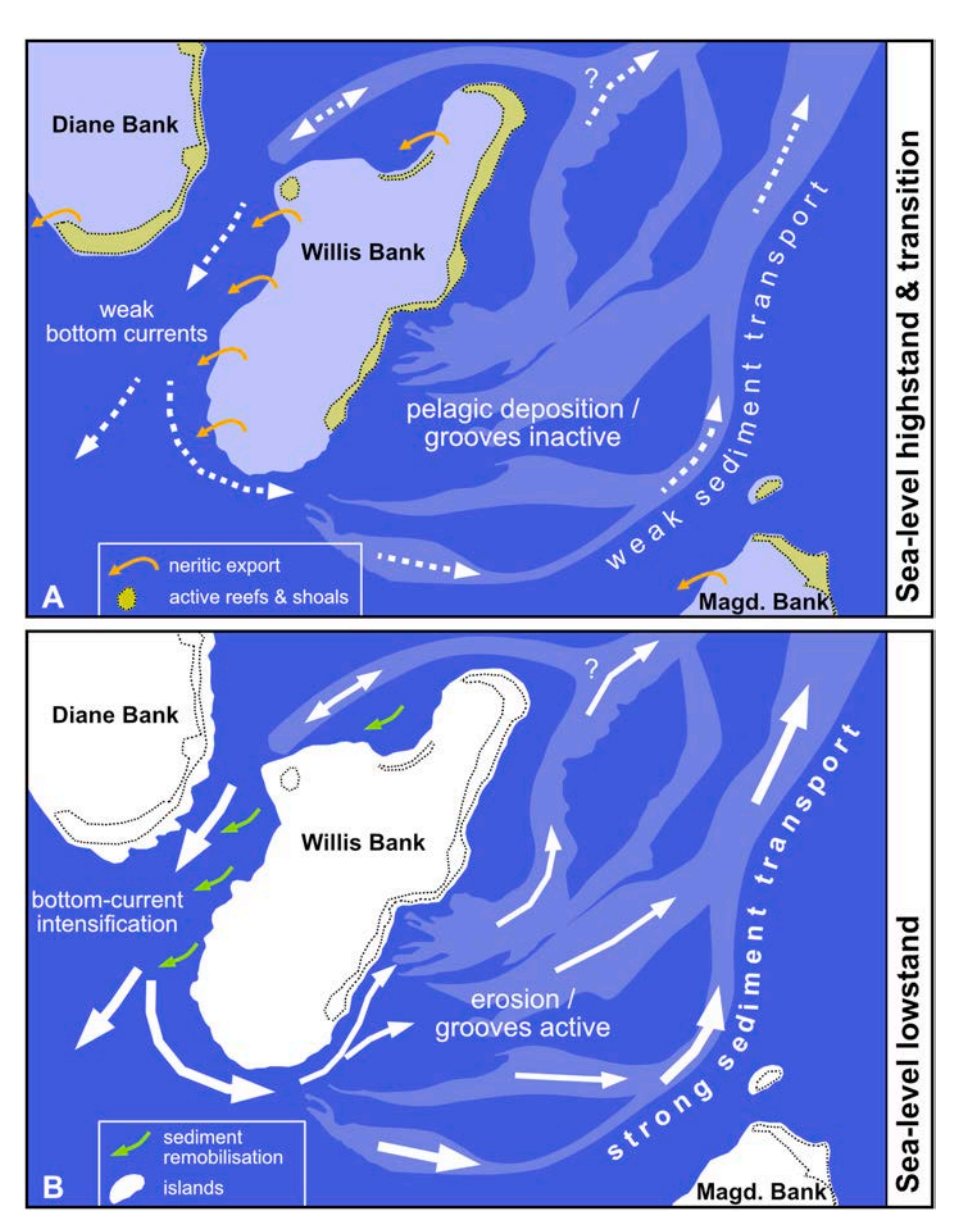


Fig. 14. Dynamics of canyon-channel system activity in Willis Passage dependent of sea-level position. A) Carbonate bank tops are flooded during sea-level highstand and mesophotic carbonate production prevails. Bottom currents in the marine passages are weak and grooves are covered by pelagic sediments. With falling sea level, there is a short peak of neritic production due to increased light availability. Sediment exported during highstand and transition accumulates near the banks; B) With sea-level falling below the bank edges, bottom currents intensify, sediment from bank-distal depocenters is resuspended, and canyons and grooves become active, nourished by sediment-laden gravity flows.

rising sea level again creates a short window of opportunity for shallow-water carbonate production including the build-up of *Halimeda* bioherms (Reolid et al., 2024). At the same time, paleosols and aeolian deposits from glacial times are reworked from the platform top, as e.g. indicated by red sediment layers in the uppermost parts of sediment cores from the slopes of Tregrosse Bank (Betzler et al., 2024a).

5.4. Age of the Willis Passage canyon-channel system

Seismic data show no buried carbonate banks or mounds in the Willis Passage, down to the acoustic basement, i.e. the middle Eocene (Fig. 10; Supplement 6). This observation contrasts with other areas of the Queensland Plateau, where buried carbonate edifices are common (Betzler et al., 2024b). The lack of buried banks in Willis Passage implies that this marine strait is a persistent feature of the Queensland Plateau, likely since the middle Eocene. The history of the canyon systems in Willis Passage, by contrast, is less continuous. While stratigraphic units I

and III are characterized by sub-horizontal strata and the lack of large cut-and-fill structures, there are extensive buried erosive structures in stratigraphic Unit II (1400 to 1000 mbsl) that likely resemble a canyon system similar to the present day C1 canyon (Fig. 10). The present canyon-channel system is therefore seen as (at least) the second generation of such a system in Willis Passage.

The timing of the first occurrence of canyons in Willis Passage (in stratigraphic Unit II) can roughly be estimated by correlating the lowest horizons of the canyon fill with dated intervals of ODP Leg 133, Site 811/825 c. 250 km west of Willis Passage (Supplement 6). This 'jump correlation' is afflicted with a high uncertainty due to the occurrence of extensive mass-transport complexes that hinder the continuous tracing of seismic horizons between the ODP site and the study area (see MTC in Supplement 6B), and therefore only gives a rough estimation. The correlation places the onset of canyon burial in the time interval between 5.3 and 8.1 Ma. Past 8 Ma, the Queensland Plateau was a wide, open platform, characterized by low-relief banks, mounds, and drift

sediments shaped by bottom currents (Betzler et al., 2024b). As a similar age was found for the onset of delta drift progradation south of Willis Bank (Fig. 13; Supplement 6C), it is hypothesized that the formation of the canyon-channel systems accompanied the onset of widespread bottom-current deposition on the Queensland Plateau.

The interplay of stratigraphic intervals with canyon incision and intervals that lack such submarine landforms indicate profound and recurring changes in the current regime of the Queensland Plateau through time. It can only be hypothesized, however, that this variability reflects the response of the local current regime to changing platform geometry over time, with active canyon-channel systems formed during stages characterized by a high-relief platform top, and burying of sediment transport paths when the platform top is open and lacks significant obstacles.

With the available data, it is not possible to date the beginning of modern canyon erosion. However, winnowing and the resulting thinning and dip of sedimentary beds towards the C1 canyon (stratigraphic Unit IV, Fig. 6) suggests that pelagic sedimentation and canyon formation acted synchronously over longer time scales. Other indicators for a long-lasting history of the present canyon-channel system comprise 1.) the erosional scarps, up to 75 m high, that flank the canyon where it cuts into the block fields near the southern tip of Willis Bank; and 2.) the presence of a thick (up to 40 m) drift sediment body composed of several packages of well stratified sediments that unconformably overly the floor of the (previously formed) canyon (Fig. 5). In summary, it appears likely that the modern canyon-channel systems of Willis Passage evolved over at least several glacial-interglacial cycles.

6. Conclusions

Slope-detached canyon-channel systems at the seafloor surrounding the carbonate banks of the Queensland Plateau are recognized as an important element of the carbonate source-to-sink system. Submarine landforms and sedimentary architecture indicate that the formation of theses canyons is controlled by sediment-laden bottom currents that propagate down-slope, in opposite direction to the prevailing ocean current regime, and are driven by gravity. The formation of these bottom currents is linked to the steep relief of the partially drowned carbonate platform, which comprises larger carbonate edifices that are separated by deep marine passages. Oceanic and tidal currents are channelized and accelerated in the narrow passages, allowing for sediment resuspension. This mechanism appears to be most active during phases of lower than present sea level, when bottom currents are assumed to intensify due to the reduced flow cross-section and the lower water depth. During sealevel highstand, by contrast, bottom currents are weaker and are restricted to the canyon, while other erosive landforms in the marine passage are inactive and covered by pelagic sediments.

We conclude that deep-water canyon-channel systems represent important sediment conduits, connecting platform-slope proximal depocenters with distal abyssal sinks. The sediment relocation in these canyons not only affects the long-term sediment budget of carbonate platforms by removing sediment from the system, but also has implications for the long-term burial of atmospheric carbon-dioxide.

CRediT authorship contribution statement

Sebastian Lindhorst: Writing – review & editing, Writing – original draft, Visualization, Validation, Supervision, Project administration, Methodology, Investigation, Funding acquisition, Formal analysis, Data curation, Conceptualization. Linus Budke: Writing – original draft, Visualization, Investigation, Formal analysis, Conceptualization. Robin J. Beaman: Writing – review & editing, Writing – original draft, Investigation, Formal analysis. Jan Oliver Eisermann: Writing – original draft, Visualization, Data curation. Christian Hübscher: Writing – original draft, Investigation, Funding acquisition, Formal analysis. Niko Lahajnar: Writing – original draft, Investigation, Formal analysis, Data

curation. **Thomas Lüdmann:** Writing – original draft, Investigation, Funding acquisition, Formal analysis, Data curation. **Jody M. Webster:** Writing – review & editing, Writing – original draft, Investigation, Formal analysis. **Christian Betzler:** Writing – review & editing, Writing – original draft, Validation, Investigation, Funding acquisition, Formal analysis, Conceptualization.

Declaration of competing interest

The authors declare the following financial interests/personal relationships which may be considered as potential competing interests:

Christian Betzler reports financial support was provided by Federal Ministry of Education and Research, Germany. If there are other authors, they declare that they have no known competing financial interests or personal relationships that could have appeared to influence the work reported in this paper.

Acknowledgements

We thank the officers and crew of RV *Sonne* for their support during Cruise SO292. The shipboard scientific party and the technicians provided the solid fundament that allow acquiring the data used in this study. The Schmidt Ocean Institute is thanked for the RV *Falkor* multibeam data acquired during cruises FK200429 and FK200802. Victoria Strehse, Johanna Becking, and Joely Maak are thanked for the onboard processing of SO292 multibeam and Parasound data. We also thank Parks Australia for the research permit for Cruise SO292 (permit EPBC 2022/9168). This study was funded by the Federal Ministry of Education and Research Germany through grant 03G0292A (ICECARB, 'Towards an understanding of carbonate platforms in the icehouse world') to CB, CH, SL, and TL. Three anonymous reviewers are thanked for their time and their thorough and constructive reviews that helped in improving our manuscript.

Appendix A. Supplementary data

Supplementary data to this article can be found online at https://doi.org/10.1016/j.margeo.2025.107678.

Data availability

SO292 multibeam, Parasound, and CTD data used for this study are available from the data depository PANGAEA: https://doi.org/10.1594/PANGAEA.965787 (EM122 multibeam bathymetry), https://doi.org/10.1594/PANGAEA.969088 (Parasound PS70), and https://doi.org/10.1594/PANGAEA.973808 (CTD).

References

AIMS, Australian Institute of Marine Science, 2024. eReefs visualisations. Hydrodynamic model GBR4 (4 km), current at 1.5 m, 18 m, and 103 m depth, Queensland, Data were extracted using eReefs extraction tool. https://extraction.ereefs.aims.gov.au/ (download on 2024.04.28, last accessed 2025.07.03).

Allen, J.R.L., 1984. Sedimentary structures – their character and physical basis (unabridged and corrected one-volume edition). Dev. Sedimentol. 30, 1256. Andrews, J.C., Clegg, S., 1989. Coral Sea circulation and transport deduced from modal

information models. Deep-Sea Res. 36, 957–974.

Bailey, L.P., Clare, M.A., Hunt, J.E., Kane, I.A., Miramontes, E., Fonnesu, M., Argiolas, R.,

Bailey, L.P., Clare, M.A., Hunt, J.E., Kane, I.A., Miramontes, E., Fonnesu, M., Argiolas, R., Malgesini, G., Wallerand, R., 2024. Highly variable deep-sea currents over tidal and seasonal timescales. Nat. Geosci. 17, 787–794.

Beaman, R.J., 2010. High-resolution depth model for the Great Barrier Reef and Coral Sea - 100 m. In: Geoscience Australia, Canberra. https://doi.org/10.26186/ 5e2f8bb629d07.

Beaman, R., Schmidt Ocean Institute, 2024. Schmidt Ocean Institute Expedition Report: Visioning the Coral Sea Marine Park, Zenodo, p. 39. https://doi.org/10.5281/zenodo.14335264. Available at: https://zenodo.org/records/14335264.

Betzler, C., Kroon, D., Gartner, S., Wei, W., 1993. Eocene to Miocene chronostratigraphy of the Queensland Plateau: control of climate and sea level on platform evolution. In: Proc. Ocean Drill. Proj., Sci. Results, 133, pp. 281–289.

Betzler, C., Artschwager, M., Becking, J., Bialik, O.M., Eggers, D., Eisermann, J.O., Falkenberg, P., Häcker, T., Hübscher, C., Hincke, C., Lahajnar, N., Lindhorst, S.,

- Lüdmann, T., Maak, J.M., Maul, J., Petrovic, A., Reolid, J., Saitz, Y., Schmidt, M.C., Schönbeck, F., Schwarz, T., Strehse, V., Wasilewski, T., Welsch, A., 2022. Towards an Understanding of Carbonate Platforms in the Icehouse World, Cruise No. SO292, 15.05.2022 21.06.2022, Nouméa (New Caledonia) Nouméa (New Caledonia), SONNE-Berichte. Begutachtungspanel Forschungsschiffe, Bonn, p. 58. https://doi.org/10.48433/cr_so292.
- Betzler, C., Lindhorst, S., Hincke, C., Eisermann, J.O., Bialik, O., Petrovic, A., Reolid, J., Beaman, R.J., Webster, J., Lüdmann, T., Hübscher, C., 2024a. Dismantling of an isolated tropical carbonate platform through flank collapse and canyon erosion, Coral Sea, Northeast Australia. Mar. Geol. 475, 107361.
- Betzler, C., Hübscher, C., Lindhorst, S., Lüdmann, T., Hincke, C., Beaman, R.J., Webster, J.M., 2024b. Seismic stratigraphic and sedimentary record of a partial carbonate platform drowning, Queensland Plateau, North-East Australia. Mar. Geol. 470, 107255.
- Black, K., Peppe, O., Gust, G., 2003. Erodibility of pelagic carbonate ooze in the Northeast Atlantic. J. Exp. Mar. Biol. Ecol. 285-286, 143–163.
- Boland, F.M., Church, J.A., 1981. The east Australian current 1978. Deep-Sea Res. 28, 937–957.
- Børve, E., Isachsen, P.E., Nøst, O.A., 2021. Rectified tidal transport in Lofoten-Vesterålen, northern Norway. Ocean Sci. 17, 1753–1773.
- Bourget, J., Zaragosi, S., Ellouz-Zimmermann, N., Mouchot, N., Garlan, T., Schneider, J. L., Lanfumey, V., Lallemant, S., 2011. Turbidite system architecture and sedimentary processes along topographically complex slopes: the Makran convergent margin. Sedimentology 58, 376–406.
- Brinkman, R., Wolanski, E., Deleersnijder, E., McAllister, F., Skirving, W., 2001. Oceanic inflow from the Coral Sea into the Great Barrier Reef. Estuar. Coast. Shelf Sci. 54, 655–668.
- Brooke, B., 2020. Marine Geoscience Data System, Cruise RV Falkor FK200802. https://www.marine-geo.org/tools/search/entry.php?id=FK200802.
- Bryant, W.R., Bean, D., Slowey, N., 2005. Mega-furrows, contour currents and density flows of the Northwest Gulf of Mexico continental slope and rise. In: Ninth International Congress of the Brazilian Geophysical Society. https://doi.org/ 10.3997/2214-4609-pdb.160.SBGF017.
- Church, J.A., 1987. East Australian current adjacent to the Great Barrier Reef. Austral. J. Mar. Freshwater Res. 38, 671–683.
- Colberg, F., Brassington, G.B., Sandery, P., Sakov, P., Aijaz, S., 2020. High and medium resolution ocean models for the Great Barrier Reef. Ocean Model 145, 101507.
- Counts, J.W., Jorry, S.J., Leroux, E., Miramontes, E., Jouet, G., 2018. Sedimentation adjacent to atolls and volcano-cored carbonate platforms in the Mozambique Channel (SW Indian Ocean). Mar. Geol. 404, 41–59.
- Davies, P.J., Symonds, P.A., Feary, D.A., Pigram, C.J., 1989. The evolution of the carbonate platforms of Northeast Australia. Soc. Econ. Paleontol. Mineral. Spec. Publ. 44, 233–258.
- Davies, P.J., McKenzie, J.A., Palmer-Julson, A., Betzler, C., Brachert, T.C., Chen, M.-P.P., Crumière, J.-P., Dix, G.R., Droxler, A.W., Feary, D.A., Gartner, S., Glenn, C.R., Isern, A., Jackson, P.D., Jarrard, R.D., Katz, M.E., Konishi, K., Kroon, D., Ladd, J.W., Martin, J.M., McNeill, D.F., Montaggioni, L.F., Muller, D.W., Omarzai, S.K., Pigram, C.J., Swart, P.K., Symonds, P.A., Watts, K.F., Wei, W., 1991. Proceedings of the Ocean Drilling Program, Initial Reports, 133. Northeast Australian Margin, College Station, Texas, p. 1496.
- Euler, T., Herget, J., 2012. Controls on local scour and deposition induced by obstacles in fluvial environments. Catena 91, 35–46.
- Feary, D.A., Champion, D.C., Bultitude, R.J., Davies, P.J., 1993. Igneous and metasedimentary basement lithofacies of the Queensland Plateau (Sites 824 and 825).
 In: Proceedings of the Ocean Drilling Program, 133. Northeast Australian Margin, College Station, Texas, p. 6.
- Flood, R.D., 1981. Distribution, morphology, and origin of sedimentary furrows in cohesive sediments, Southampton Water. Sedimentology 28, 511–529.
- Flood, R.D., 1983. Classification of sedimentary furrows and a model for furrow initiation. Geol. Soc. Am. Bull. 94, 630–639.
- Flood, R.D., Hiscott, R.N., Aksu, A.E., 2009. Morphology and evolution of an anastomosed channel network where saline underflow enters the Black Sea. Sedimentology 56, 807–839.
- Gardner, T.W., 1983. Experimental study of knickpoint and longitudinal profile evolution in cohesive, homogeneous material: Discussion and reply. Geol. Soc. Am. Bull. 94, 664–672.
- Gardner, J.V., Peakall, J., Armstrong, A.A., Calder, B.R., 2020. The geomorphology of submarine channel systems of the Northern Line Islands Ridge, central equatorial Pacific Ocean. Front. Earth Sci. 8, 87.
- Gasparin, F., Maes, C., Sudre, J., Garcon, V., Ganachaud, A., 2014. Water mass analysis of the Coral Sea through an Optimum Multiparameter method. J. Geophys. Res. Oceans 119, 7229–7244.
- Grant, K.M., Rohling, E.J., Bronk Ramsey, C., Cheng, H., Edwards, R.L., Florindo, F., Heslop, D., Marra, F., Roberts, A.P., Tamisiea, M.E., Williams, F., 2014. Sea-level variability over five glacial cycles. Nat. Commun. 5, 5076.
- Grimaud, J.-L., Paola, C., Voller, V., 2015. Experimental migration of knickpoints: Influence of style of base-level fall and bed lithology. Earth Surface Dynam. Discus. 3, 773–805.
- Habgood, E.L., Kenyon, N.H., Masson, D.G., Akhmetzhanov, A., Weaver, P.P.E., Gardner, J., Mulder, T., 2003. Deep-water sediment wave fields, bottom current sand channels and gravity flow channel-lobe systems: Gulf of Cadiz, NE Atlantic. Sedimentology 50, 483–510.
- Heijnen, M.S., Clare, M.A., Cartigny, M.J.B., Talling, P.J., Hage, S., Lintern, D.G., Stacey, C., Parsons, D.R., Simmons, S.M., Chen, Y., Sumner, E.J., Dix, J.K., Hughes Clarke, J.E., 2020. Rapidly-migrating and internally-generated kniickpoints can control submarine channel evolution. Nat. Commun. 11, 3129.

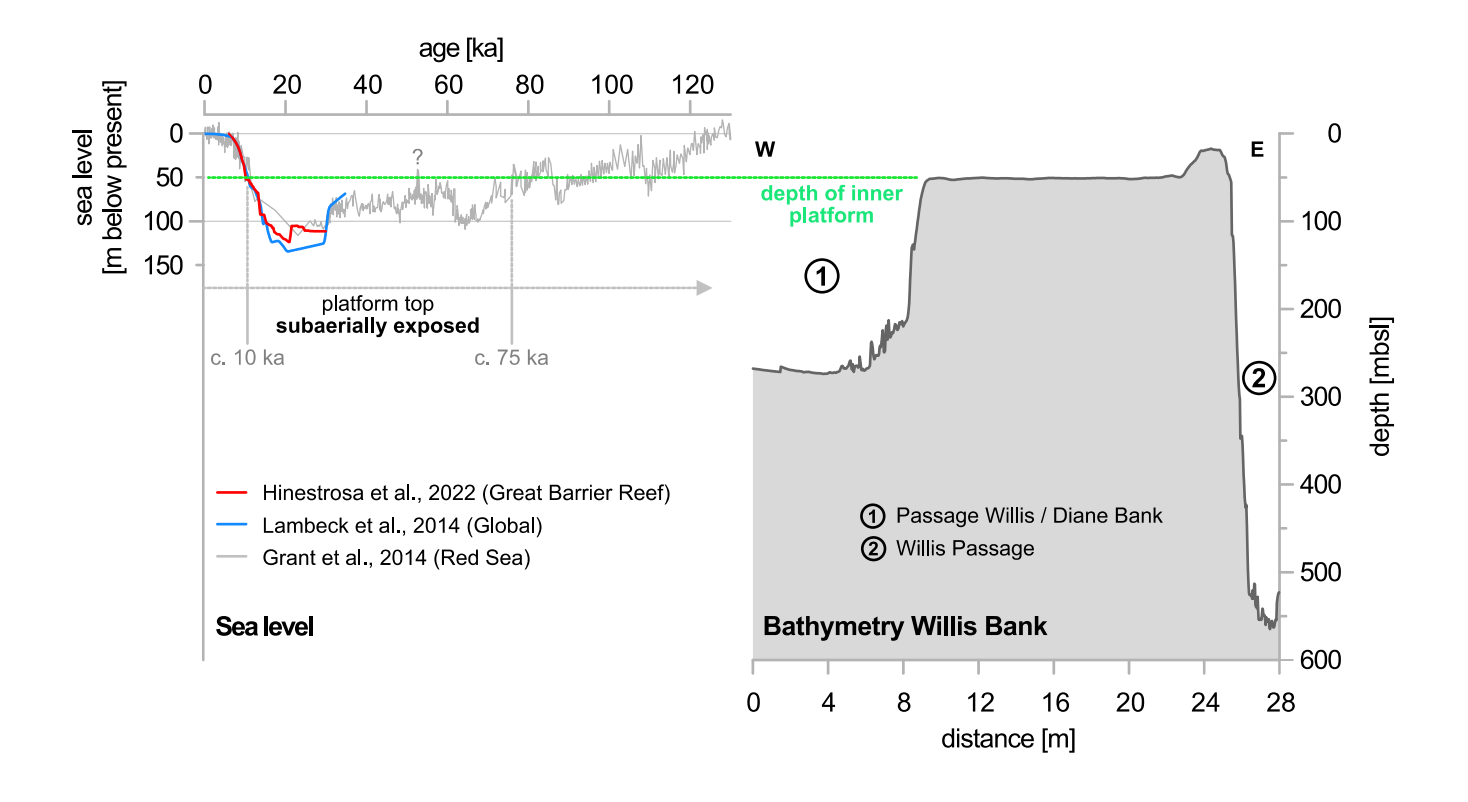
Heijnen, M.S., Clare, M.A., Cartigny, M.J.B., Talling, P.J., Hage, S., Pope, E.L., Bailey, L., Sumner, E., Lintern, D.G., Stacey, C., Parsons, D.R., Simmons, S.M., Chen, Y., Hubbard, S.M., Eggenhuisen, J.T., Kane, I., Hughes Clarke, J.E., 2022. Fill, flush or shuffle: How is sediment carried through submarine channels to build lobes? Earth Planet. Sci. Lett. 584, 117481.

- Hernández-Molina, F.J., Llave, E., Stow, D.A.V., García, M., Somoza, L., Vázquez, J.T., Lobo, F., Maestro, A., Díaz del Río, V., León, R., Medialdea, T., Gardner, J., 2006. The contourite depositional system of the Gulf of Cadiz: a sedimentary model related to the bottom current activity of the Mediterranean Outflow Water and the continental margin characteristics. Deep-Sea Res. Part II Top. Stud. Oceanogr. 53, 1420–1463.
- Hinestrosa, G., Webster, J.M., Beaman, R.J., 2022. New constraints on the postglacial shallow-water carbonate accumulation in the Great Barrier Reef. Sci. Report. 12, 924
- Imran, J., Islam, M.A., Huang, H., Kassem, A., Dickerson, J., Pirmez, C., Parker, G., 2007.
 Helical flow couplets in submarine gravity underflows. Geology 35, 659–662.
- Jorry, S.J., Jouet, G., Edinger, E.N., Toucanne, S., Counts, J.W., Miramontes, E., Courgeon, S., Riveiros, N.V., Le Roy, P., Camoin, G.F., 2020. From platform top to adjacent deep sea: New source-to-sink insights into carbonate sediment production and transfer in the Southwest Indian Ocean (Glorieuses archipelago). Mar. Geol. 423, 106144.
- Kessler, W.S., Cravatte, S., 2013. Mean circulation of the Coral Sea. J. Geophys. Res. 118, 6385–6410.
- Kongsberg Maritime, 2011. Kongsberg EM 122 Multibeam Echo Sounder. Product Description. Kongsberg Maritime AS, p. 56.
- Konsoer, K., Zinger, J., Parker, G., 2013. Bankfull hydraulic geometry of submarine channels created by turbidity currents: Relations between bankfull channel characteristics and formative flow discharge. J. Geophys. Res. Earth Surf. 118, 216–228.
- Lambeck, K., Rouby, H., Purcell, A., Sun, Y., Sambridge, M., 2014. Sea level and global ice volumes from the Last Glacial Maximum to the Holocene. In: Proceedings of the National Academy of Science, U.S.A, 43, pp. 15296–15303.
 Lee, S.E., Talling, P.J., Ernst, G.G.J., Hogg, A.J., 2002. Occurrence and origin of
- Lee, S.E., Talling, P.J., Ernst, G.G.J., Hogg, A.J., 2002. Occurrence and origin of submarine plunge pools at the base of the US continental slope. Mar. Geol. 185, 363–377.
- Lüdmann, T., Betzler, C., Eberli, G.P., Reolid, J., Reijmer, J.J.G., Sloss, C.R., Bialik, O.M., Alvarez-Zarikian, C.A., Alonso-García, M., Blättler, C.L., Guo, J.A., Haffen, S., Horozal, S., Inoue, M., Jovane, L., Kroon, D., Lanci, L., Laya, J.C., Mee, A.L.H., Nakakuni, M., Nath, N., Niino, K., Petruny, L.M., Pratiwi, S.D., Slagle, A.L., Su, X., Swart, P.K., Wright, J.D., Yao, Z., Young, J.R., 2018. Carbonate delta drift: a new sediment drift type. Mar. Geol. 401, 98–111.
- Lüdmann, T., Betzler, C., Lindhorst, S., Lahajnar, N., Hübscher, C., 2022a. Submarine landsliding in carbonate ooze along low-angle slopes (Inner Sea, Maldives). Mar. Pet. Geol. 136. 105403.
- Lüdmann, T., Betzler, C., Lindhorst, S., 2022b. The Maldives, a key location of carbonate drifts. Mar. Geol. 450, 106838.
- McArthur, A.D., McCaffrey, W.D., 2018. Sedimentary architecture of detached deepmarine canyons: examples from the East Coast Basin of New Zealand. Sedimentology 66. 1067–1101.
- Meiburg, E., Kneller, B., 2010. Turbidity currents and their deposits. Annu. Rev. Fluid Mech. 42, 135–156.
- Menard, H.W., 1955. Deep-sea channels, topography, and sedimentation. Am. Assoc. Pet. Geol. Bull. 39, 236–255.
- Micallef, A., Ribó, M., Canals, M., Puig, P., Lastras, G., Tubau, X., 2014. Space-for-time substitution and the evolution of a submarine canyon-channel system in a passive progradational margin. Geomorphology 221, 34–50.
- Miramontes, E., Jouet, G., Thereau, E., Bruno, M., Penven, P., Guerin, C., Le Roy, P., Droz, L., Jorry, S.J., Hernández-Molina, F.J., Thiéblemont, A., Silva Jacinto, R., Cattaneo, A., 2020. The impact of internal waves on upper continental slopes: insights from the Mozambican margin (Southwest Indian Ocean). Earth Surf. Process. Landf. 45, 1469–1482.
- Mosher, D.C., 2011. Cautionary considerations for geohazard mapping with multibeam sonar: resolution and the need for the third and fourth dimensions. Mar. Geophys. Res. 32, 25–35.
- Mulder, T., Gillet, H., Hanquiez, V., Ducassou, E., Fauquembergue, K., Principaud, M., Conesa, G., Le Goff, J., Ragusa, J., Bashah, S., Bujan, S., Reijmer, J.J.G., Cavailhes, T., Droxler, A.W., Blank, D.G., Guiastrennec, L., Fabregas, N., Recouvreur, A., Seibert, C., 2017. Carbonate slope morphology revealing a giant submarine canyon (Little Bahama Bank, Bahamas). Geology 46, 31–34.
- Mulder, T., Gillet, H., Hanquiez, V., Reijmer, J.J.G., Droxler, A.W., Recouvreur, A., Fabregas, N., Cavailhes, T., Fauquembergue, K., Blank, D.G., Guiastrennec, L., Seibert, C., Bashah, S., Bujan, S., Ducassou, E., Principaud, M., Conesa, G., Le Goff, J., Ragusa, J., Busson, J., Borgomano, J., 2019. Into the deep: a coarse-grained carbonate turbidite valley and canyon in ultra-deep carbonate setting. Mar. Geol. 407. 316–333.
- Mulder, T., Cavailhes, T., Hanquiez, V., Gillet, H., Recouvreur, A., Fabregas, N., 2022. Giant deep submarine depressions: a combined dissolution-mechanical process along carbonate margins. GSA Bull. 135, 743–752.
- Mullins, H.T., Neumann, A.C., Wilber, R.J., Hine, A.C., Chinburg, S.J., 1980. Carbonate sediment drifts in the northern Straits of Florida. Am. Assoc. Pet. Geol. Bull. 64, 1701–1717.
- Mutter, J.C., 1977. The Queensland Plateau. Bur. Min. Resour. Geol. Geophys. Bull. 179, 1–55.
- Normandeau, A., Dafoe, L.T., Li, M.Z., Campbell, D.C., Jenner, K.A., 2024. Sedimentary record of bottom currents and internal tides in a modern highstand submarine canyon head. Sedimentology 71, 1061–1083.

Orme, G.R., 1977. The Coral Sea Plateau - a major reef province. In: Jones, O.A., Endean, R. (Eds.), Biology and Geology of Coral Reefs. Academic Press, New York, np. 267–306

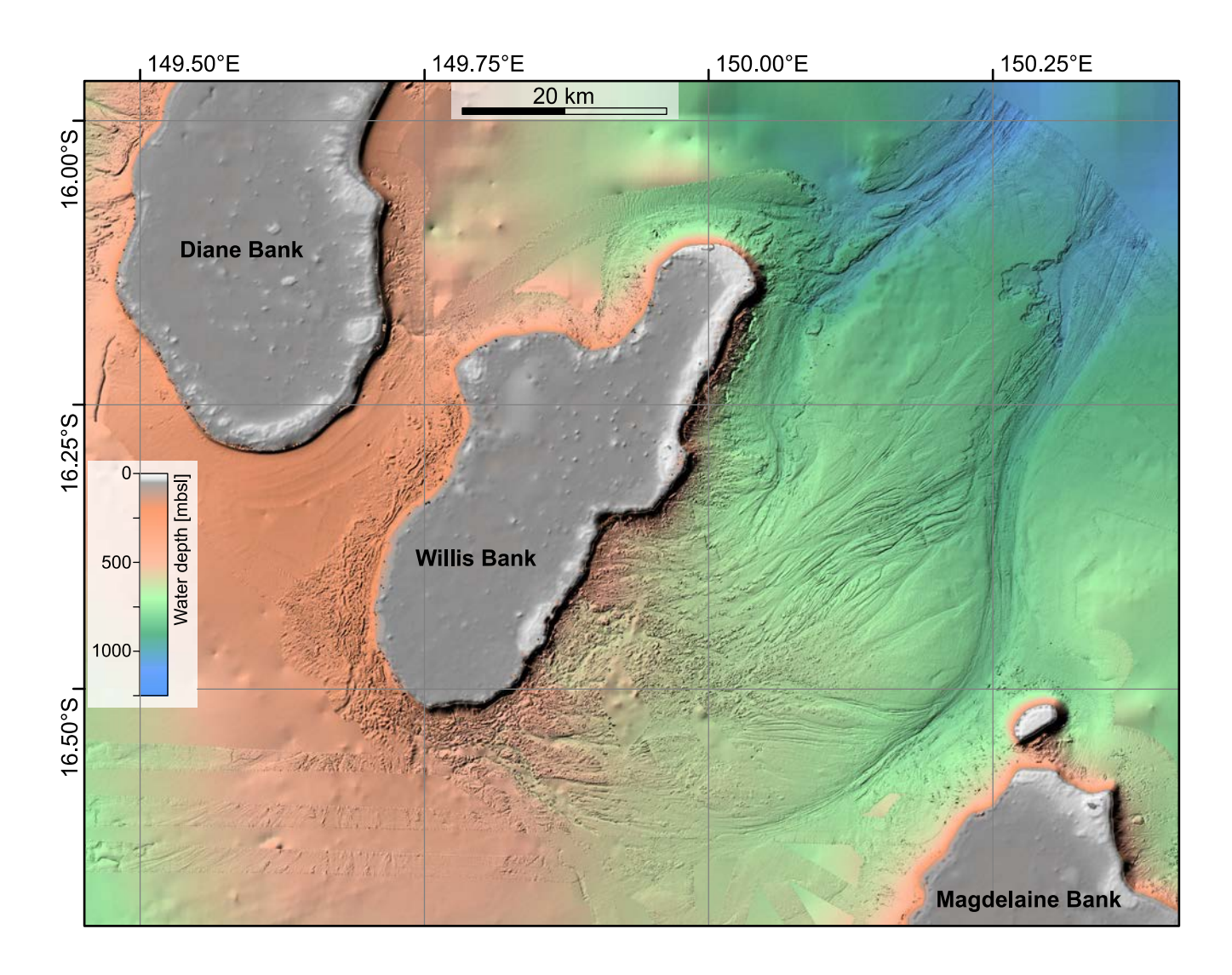
- Payros, A., Pujalte, V., 2008. Calciclastic submarine fans: an integrated overview. Earth Sci. Rev. 86, 203–246.
- Peakall, J., 2015. Undersea river patterns. Nat. Geosci. 8, 663-664.
- Peakall, J., Sumner, E.J., 2015. Submarine channel flow processes and deposits: a process-product perspective. Geomorphology 244, 95–120.
- Prager, E.J., Southard, J.B., Vivoni-Gallart, E.R., 1996. Experiments on the entrainment threshold of well-sorted and poorly sorted carbonate sands. Sedimentology 43, 33–40.
- Puga-Bernabéu, A., Webster, J.M., Beaman, R.J., Guilbaud, V., 2011. Morphology and controls on the evolution of a mixed carbonate-siliciclastic submarine canyon system, Great Barrier Reef margin, North-Eastern Australia. Mar. Geol. 289, 100–116.
- Puga-Bernabéu, A., Webster, J.M., Beaman, R.J., Guilbaud, V., 2013. Variation in canyon morphology on the Great Barrier Reef margin North-Eastern Australia: the influence of slope and barrier reefs. Geomorphology 191, 35–50.
- Rebesco, M., Hernández-Molina, F.J., Van Rooij, D., Wåhlin, A., 2014. Contourites and associated sediments controlled by deep-water circulation processes: State-of-the-art and future considerations. Mar. Geol. 352, 111–154.
- Reolid, J., Bialik, O.M., Lindhorst, S., Eisermann, J.O., Petrovic, A., Hincke, C., Beaman, R.J., Webster, J.M., Betzler, C., 2024. A new type of Halimeda bioherm on the Queensland Plateau, NE Australia. Coral Reefs 43, 801–821.
- Sandery, P., Brassington, G., Colberg, F., Herzfeld, M., Sakov, P., Maes, C., Tuteja, N., 2019. An ocean reanalysis of the western Coral Sea and Great Barrier Reef. Ocean Model 144, 101495.
- Saruwatari, A., Ingram, D.M., Cradden, L., 2013. Wave-current interaction effects on marine energy converters. Ocean Eng. 73, 106–118.
- Schiller, A., Herzfeld, M., Brinkman, R., Rizwi, F., Andrewartha, J., 2015. Cross-shelf exchanges between the Coral Sea and the Great Barrier Reef lagoon determined from a regional-scale numerical model. Cont. Shelf Res. 109, 150–163.

- Schlager, W., 2005. Carbonate sedimentology and sequence stratigraphy. In: SEPM Concepts in Sedimentology and Paleontology, 8, p. 200.
- Shaanan, U., Rosenbaum, G., Hoy, D., Mortimer, N., 2018. Late Paleozoic geology of the Queensland Plateau (offshore northeastern Australia). Aust. J. Earth Sci. 65, 357-366
- Shanmugam, G., 2003. Deep-marine tidal bottom currents and their reworked sands in modern and ancient submarine canyons. Mar. Pet. Geol. 20, 471–491.
- Shepard, F.P., 1981. Submarine canyons: Multiple causes and long-time persistence. In: American Association of Petroleum Geologist Bulletin, 65, pp. 1062–1077.
- Southard, J.B., Young, R.A., Hollister, C.D., 1971. Experimental erosion of calcareous ooze. J. Geophys. Res. 76, 5903–5909.
- Stow, D.A.V., Hernández-Molina, F.J., Llave, E., Sayago-Gil, M., Díaz del Río, V., Branson, A., 2009. Bedform-velocity matrix: the estimation of bottom current velocity from bedform observations. Geology 37, 327–330.
- Stow, D.A.V., Hernández-Molina, F.J., Llave, E., Bruno, M., García, M., Díaz del Río, V., Somoza, L., Brackenridge, R.E., 2013. The Cadiz contourite channel: sandy contourites, bedforms and dynamic current interaction. Mar. Geol. 343, 99–114.
- Watson, S.J., Whittaker, J.M., Lucieer, V., Coffin, M.F., Lamarche, G., 2017. Erosional and depositional processes on the submarine flanks of Ontong Java and Nukumanu atolls, western equatorial Pacific Ocean. Mar. Geol. 392, 122–139.
- Wolanski, E., 1982. Low-level trade winds over the western Coral Sea. J. Appl. Meteorol. Climatol. 21, 881–882.
- Wynn, R.B., Cronin, B.T., Peakall, J., 2007. Sinuous deep-water channels: genesis, geometry and architecture. Mar. Pet. Geol. 24, 341–387.
- Wyrtki, K., 1962. The subsurface water masses in the western South Pacific Ocean. Austral. J. Mar. Freshwater Res. 13, 18–47.
- Yu, K., Lefebvre, A., Li, W., Zhan, W., Miramontes, E., 2022. Channel inception through bottom-current erosion of pockmarks revealed by numerical simulation. Earth Surf. Process. Landf. 48, 2246–2259.



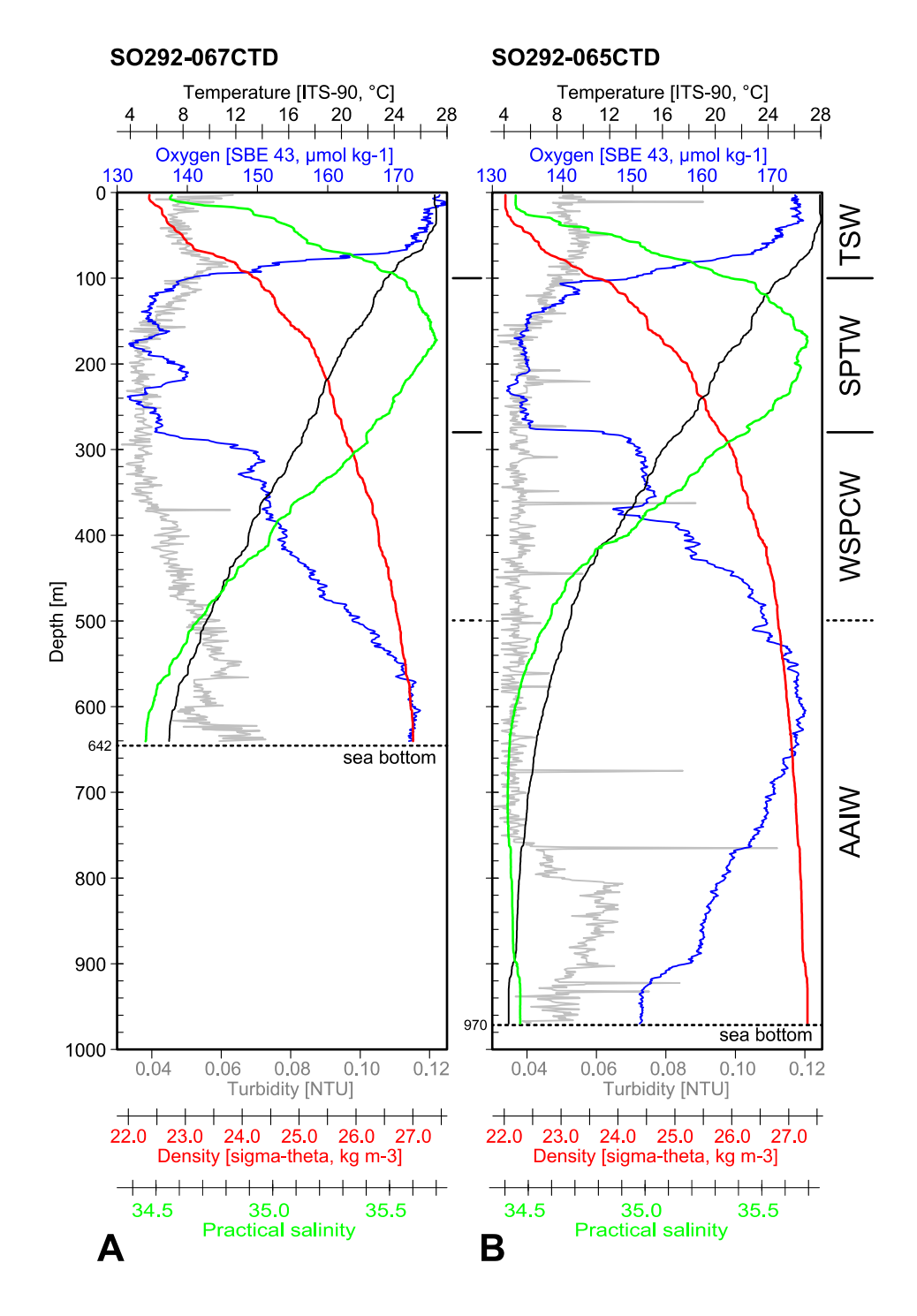
Lindhorst et al., Deep-water canyon-channel systems of the Queensland Plateau, northeast Australia

Supplement 1. Correlation of Willis Bank bathymetric cross section with late Pleistocene to Recent sea-level development. Green line indicates average depth of inner platform. Sea-level data are from Lambeck et al. (2014; global), Hinestrosa et al. (2022, Great Barrier Reef, Australia), and Grant et al. (2014, Red Sea).



Lindhorst et al., Deep-water canyon-channel systems of the Queensland Plateau, northeast Australia

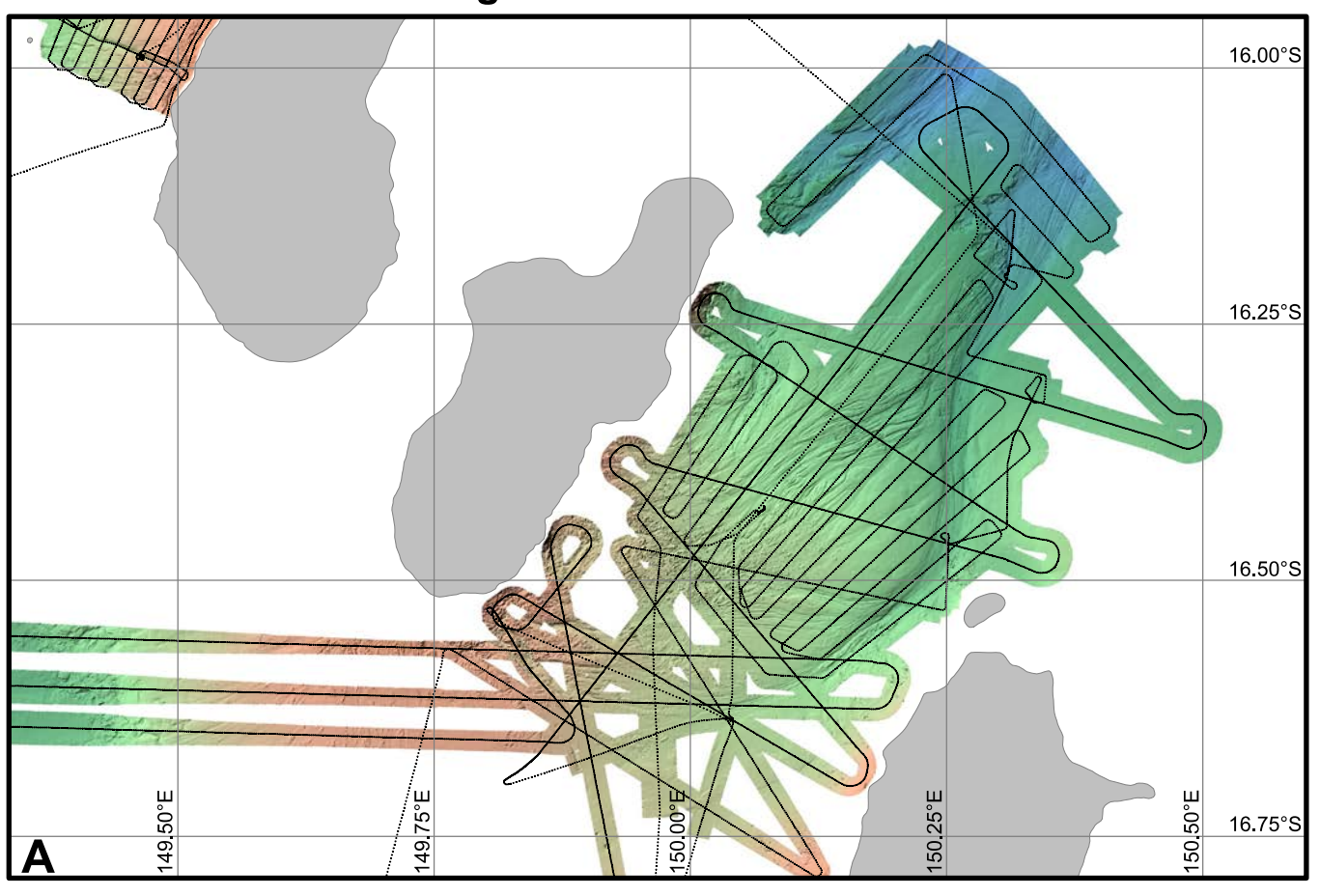
Supplement 2. Multibeam bathymetry presented in Figure 2A (see there for labels). Bathymetric data is from RV *Sonne* cruise SO292 (this study), gbr100 bathymetry (Beaman, 2010), RV *Falkor* cruises FK200802 and FK200429 (Brooke, 2020; Beaman & Schmidt Ocean Institute, 2024).



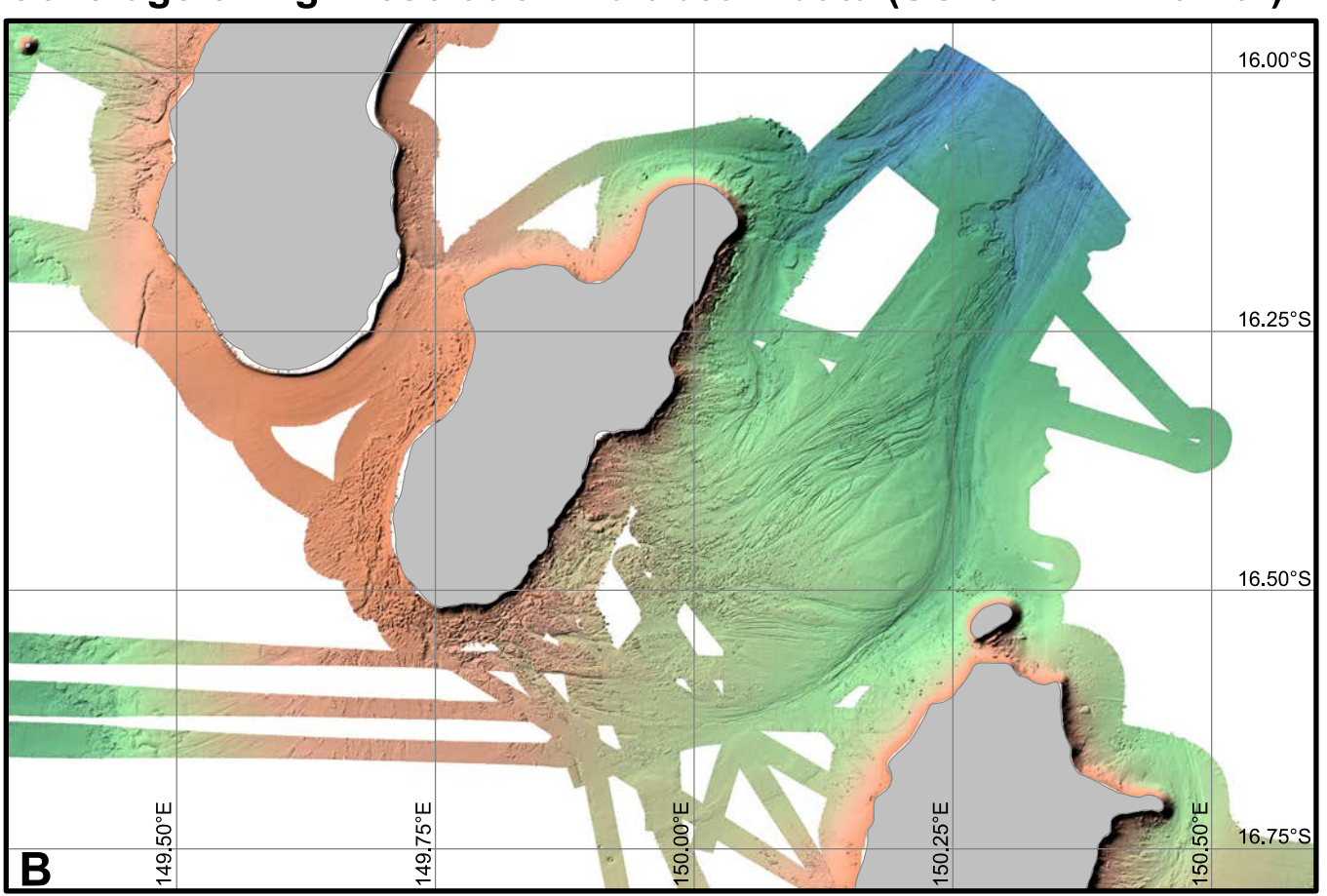
Lindhorst et al., Deep-water canyon-channel systems of the Queensland Plateau, northeast Australia

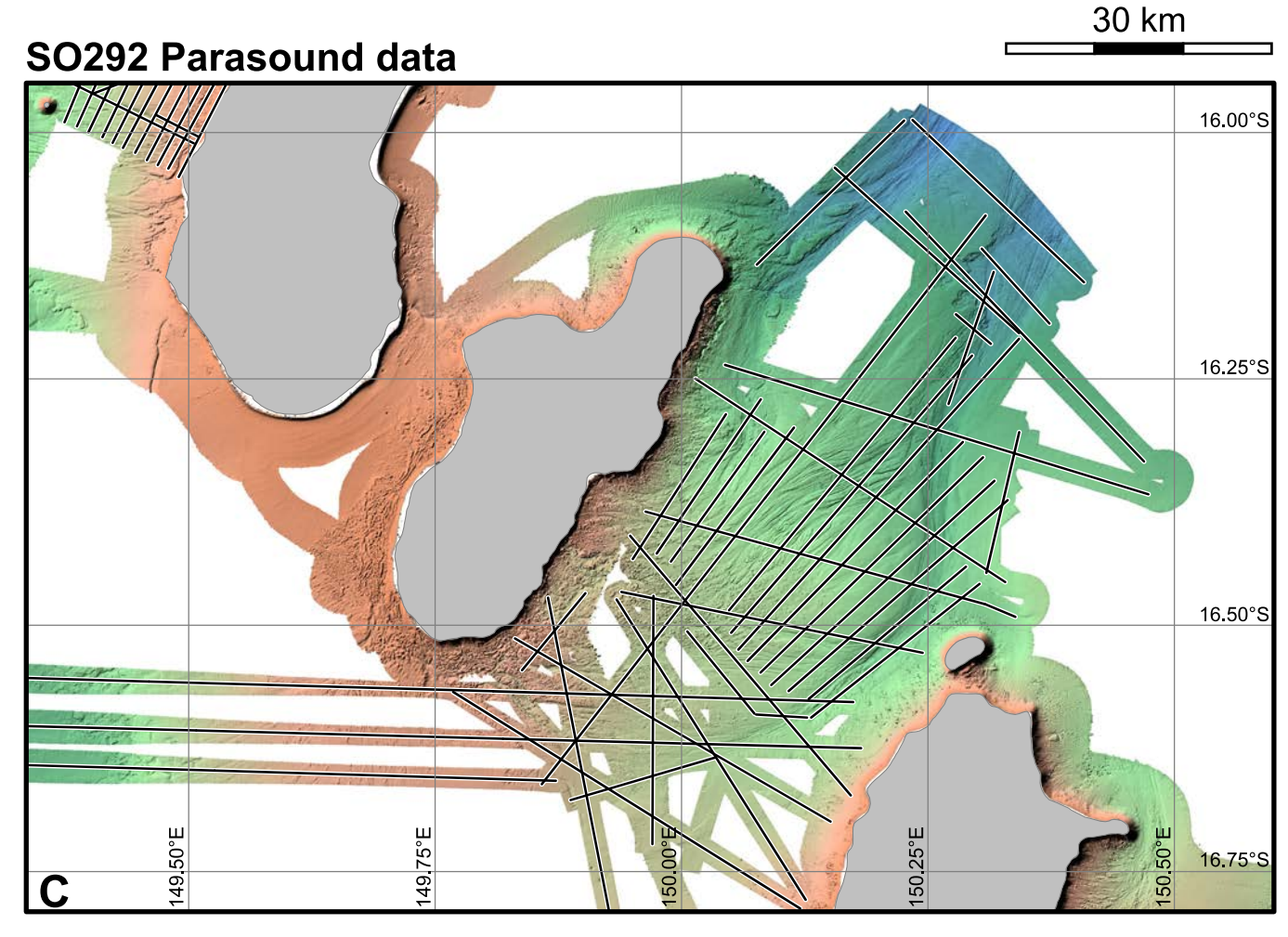
Supplement 3. Water column profiles from stations SO292-65CTD and SO292-67CTD including temperature, oxygen content, turbidity (NTU: nephelometric turbidity unit, see methods), density (sigma-theta), and salinity. See Figure 1 for locations. Oceanographic data were acquired using the RV *Sonne* shipboard CTD (conductivity-temperature-depth, SBE 911plus, Sea-Bird Electronic Inc, USA). For details see Betzler et al. (2022).

SO292 track and coverage of SO292 Multibeam data



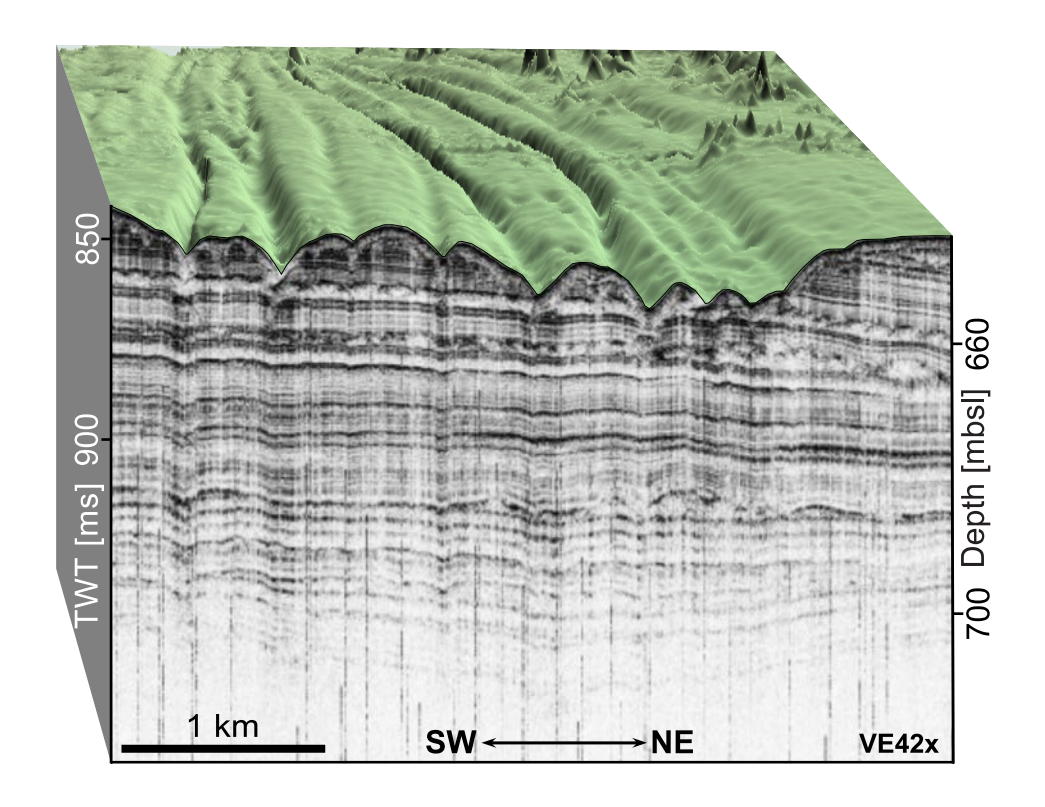
Coverage of high-resolution Multibeam data (SO292 + RV Falkor)





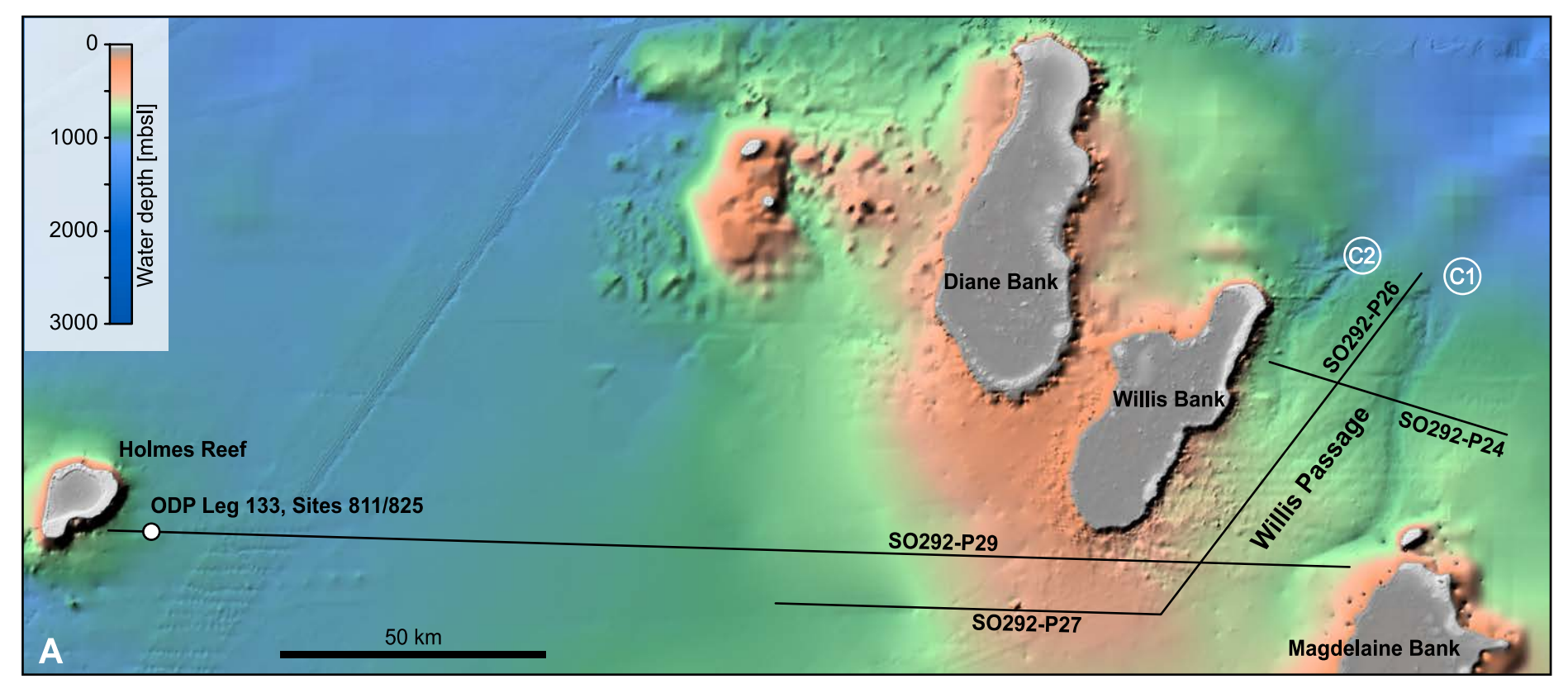
Lindhorst et al., Deep-water canyon-channel systems of the Queensland Plateau, northeast Australia

Supplement 4. Coverage of geophysical datasets used for this study. **A)** Track of RV *Sonne* cruise SO292 and coverage of multibeam data (Kongsberg EM122) acquired during this cruise; **B)** Combined multibeam data acquired during cruise SO292 and the two cruises of RV *Falkor* FK200429 and FK200802 (see methods). Gaps in the merged dataset have been filled for visualization using data of the gbr100 bathymetry (see methods); **C)** Parasound sediment echosounder (Atlas PS70) profiles acquired during RV *Sonne* cruise SO292.

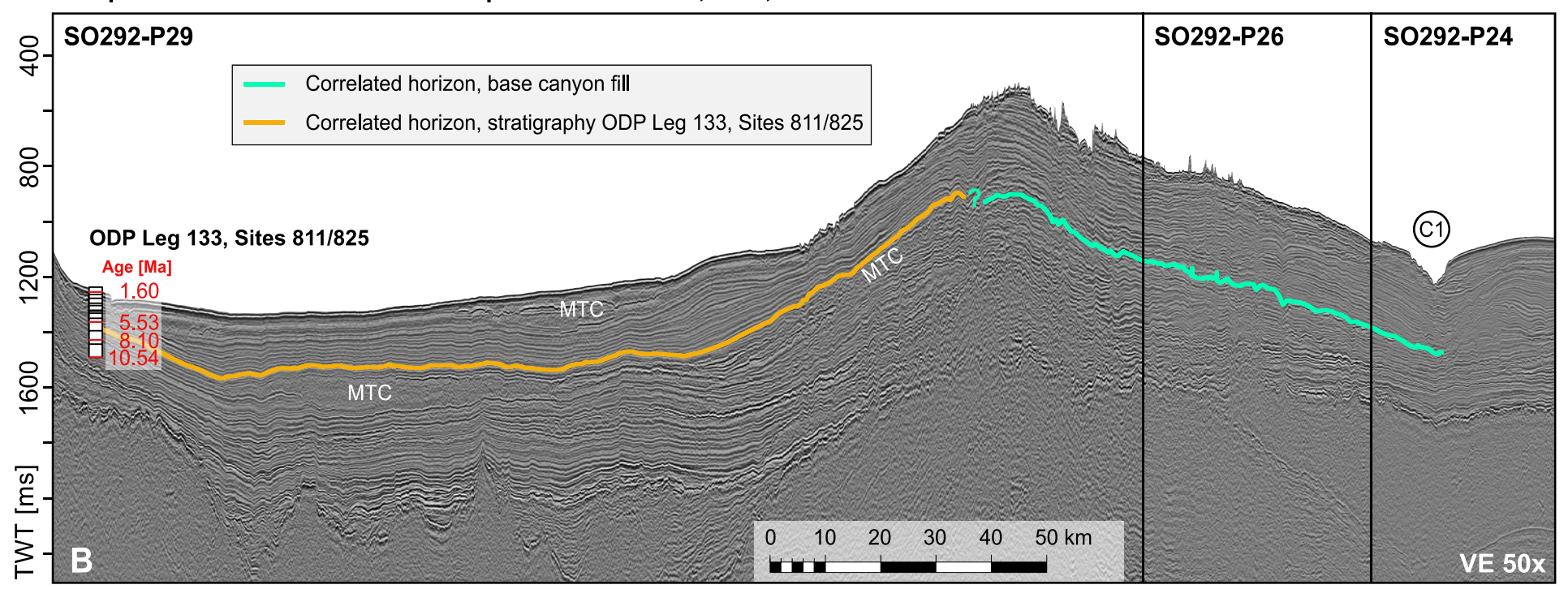


Lindhorst et al., Deep-water canyon-channel systems of the Queensland Plateau, northeast Australia

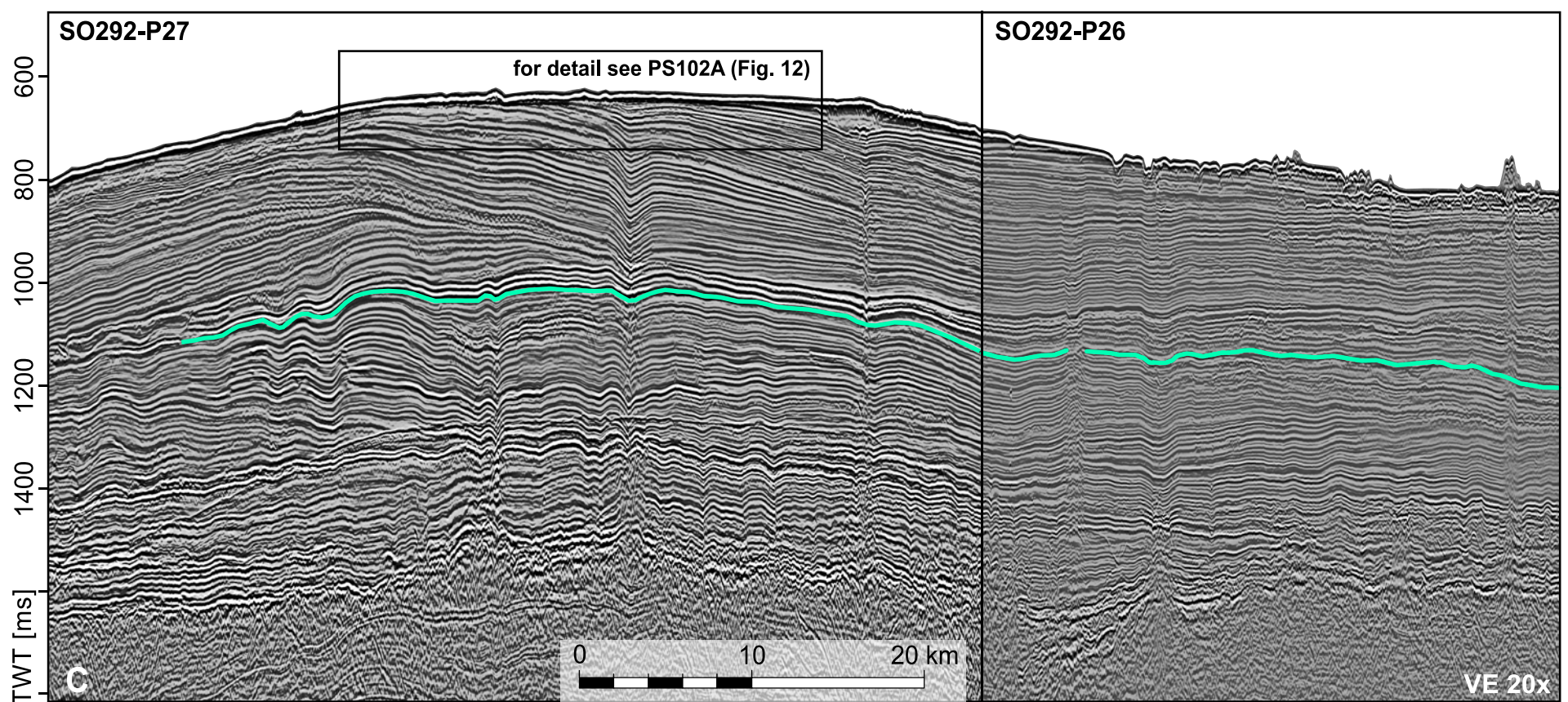
Supplement 5. Blend of multibeam bathymetry with Parasound data showing the sedimentary architecture of the linear seafloor cuts (grooves). Parasound data represent the first half of line SO292-PS144 (see Fig. 7 for location and text for discussion).



Composite of multi-channel seismic profile SO292-P29, -P26, -P24



Composite of multi-channel seismic profile SO292-P27, -P26



Lindhorst et al., Deep-water canyon-channel systems of the Queensland Plateau, northeast Australia

Supplement 6. Correlation of the seismic horizon at the basal fill of the buried canyon. Stratigraphy is from ODP Leg 133, Sites 811/825 (Davies et al., 1991). Red numbers are ages in Ma: MTC: mass-transport complexes; C1: canyon-channel system C1; see text for further explanation and discussion and Figure 1E for location of ODP site.